Bergische Universität Wuppertal

Fakultät für Mathematik und Naturwissenschaften

Institute of Mathematical Modelling, Analysis and Computational Mathematics (IMACM)

Preprint BUW-IMACM 26/16

F. Kasolis, T. Reis, M. Günther, M. Clemens, N. Haussmann

A Structure-Preserving Formulation for Coupled Field-Line Systems

July 7, 2026

http://www.imacm.uni-wuppertal.de

Mathematical Modelling and Numerical Analysis Will be set by the publisher
Modélisation Mathématique et Analyse Numérique

A STRUCTURE-PRESERVING FORMULATION FOR COUPLED FIELD-LINE SYSTEMS *

F. Kasolis[1], T. Reis[2], M. Günther[1], M. Clemens[3] and N. Haussmann[3]

Abstract. We develop a structure-preserving formulation for the coupling of a two-dimensional electromagnetic field with a reduced transmission-line model embedded in the field domain. The interaction is motivated by a distributed port that identifies the longitudinal voltage gradient with the tangential electric field along the embedded curve and leads to a current-field realization. A closed operator realization on the physical energy space is constructed, and the associated Green identity yields a boundary triplet describing the outer Maxwell port and a scalar cable port. Maximally dissipative boundary relations generate strongly continuous contraction semigroups. An implicit midpoint rule and a compatible mixed finite element discretization preserve the port-Hamiltonian interconnection structure and satisfy an exact discrete power balance. Numerical experiments for a half-wave dipole antenna illustrate the coupled dynamics and the energy behavior of the method.

Résumé. Nous développons une formulation préservant la structure pour le couplage d'un champ électromagnétique bidimensionnel avec un modèle réduit de ligne de transmission incorporé dans le domaine du champ. L'interaction est motivée par un port distribué qui identifie le gradient longitudinal de la tension au champ électrique tangent le long de la courbe immergée, conduisant ainsi à une réalisation courant–champ. Une réalisation opératorielle fermée sur l'espace d'énergie physique est construite, et l'identité de Green associée fournit un triplet de bord décrivant le port extérieur de Maxwell ainsi qu'un port scalaire de type câble. Des relations de bord maximalement dissipatives engendrent des semi-groupes de contractions fortement continus. Une discrétisation en temps par la règle du point milieu implicite, combinée à une discrétisation spatiale compatible par éléments finis mixtes, préserve la structure d'interconnexion port-hamiltonienne et satisfait un bilan de puissance discret exact. Des expériences numériques consacrées à une antenne dipôle demi-onde illustrent la dynamique du système couplé ainsi que le comportement énergétique de la méthode.

2020 Mathematics Subject Classification. 35Q61, 47A20, 47D06, 65N30, 78M10, 93C20.

The dates will be set by the publisher.

Keywords and phrases: Maxwell equations, embedded transmission lines, boundary triplets, maximal dissipativity, port Hamiltonian systems, structure preserving finite element discretization

* *This work was funded by the Deutsche Forschungsgemeinschaft (DFG, German Research Foundation) – Project-ID 531152215 – CRC 1701.*

[1] Department of Mathematics and Informatics, University of Wuppertal, Wuppertal, Germany;
e-mail: kasolis@uni-wuppertal.de & e-mail: guenther@uni-wuppertal.de.

[2] Chair of Systems Theory and Partial Differential Equations, Technische Universtität Ilmenau, Ilmenau, Germany;
e-mail: timo.reis@tu-ilmenau.de.

[3] Chair of Electromagnetic Theory, University of Wuppertal, Wuppertal, Germany;
e-mail: clemens@uni-wuppertal.de & e-mail: haussmann@uni-wuppertal.de.

Introduction

Electromagnetic field problems involving thin conductors appear in a wide range of applications, including antenna modeling, power transmission, plasma discharges, and electromagnetic compatibility analysis. Often, the conductor radius is much smaller than the characteristic length scales of the surrounding electromagnetic field, making a volumetric resolution of the conductor inefficient. A common alternative is to represent such structures by one-dimensional models embedded in the field domain. In antenna theory and thin-wire electromagnetics, this leads to hybrid field-line descriptions in which Maxwell's equations govern the surrounding field, while the conductor dynamics is reduced to line-supported variables [1, 2]. Similarly, distributed transmission line models based on the telegrapher equations describe the evolution of current and voltage along filamentary conductors [3]. Such models provide an effective macroscopic description of resistive, inductive, capacitive, and leakage effects along the line, while avoiding a full volumetric resolution of the conductor.

The analytical difficulty in such coupled models is that the interaction takes place on a lower-dimensional set inside the field domain. In particular, the tangential restriction of an $H(\mathrm{curl}, \Omega)$ field to an embedded curve is not a bounded trace operator on the electromagnetic energy space. Moreover, a line-supported current may give rise to a jump of the magnetic field across the embedded curve. Thus, the formal energy balance of the coupled equations has to be complemented by a closed operator realization on the physical energy space. One of the main purposes of this work is to provide such a realization and to identify the corresponding Maxwell and cable boundary ports through a boundary triplet.

0.1. **Compatible finite element methods**

Maxwell's equations possess a geometric structure encoded by the de Rham complex [4, 5]. In finite element discretizations this structure is mirrored by compatible discrete spaces that preserve the underlying differential relations at the discrete level [6,7]. In particular, Nédélec edge elements [8,9] provide conforming approximations of $H(\mathrm{curl}, \Omega)$ and are therefore the natural choice for the electric field in mixed formulations of Maxwell's equations [4, 10].

The field-line coupling considered here imposes an additional compatibility requirement: the tangential electric field has to be evaluated along the embedded curve. If this curve is aligned with mesh edges, the coupling can be represented directly by the edge degrees of freedom of the Nédélec space. This avoids an additional interpolation of the trace and leads to a discrete coupling operator that is power-conjugate to its transpose in the finite-dimensional port-Hamiltonian system.

0.2. **The port-Hamiltonian viewpoint**

Port-Hamiltonian systems provide a systematic framework for representing energy storage, dissipation, and power-conserving interconnection in network and distributed-parameter systems [11–13]. It is therefore well suited for coupled field-line systems, where energy is exchanged between an electromagnetic field, a line model, boundary ports, and distributed sources.

In the present work, the coupled weak formulation is first shown to admit a port-Hamiltonian power balance. This formal structure identifies the storage, dissipative, and interconnection terms, but it does not by itself yield a closed generator on the physical energy space. The operator-theoretic part is inspired by the Maxwell–cable framework developed in [14]. Compared with that work, we focus on a two-dimensional transverse-electric field-line model and combine the boundary-triplet realization with an implicit midpoint scheme and a compatible mixed finite element discretization.

In the present setting, the closed operator realization is constructed by treating the interior tangential trace as a closed operator and by using an adjoint magnetic-field–cable block. The resulting Green identity leads to a boundary triplet, through which conservative and dissipative boundary closures can be characterized. This also provides the reference structure for the time and space discretizations, which are designed to retain the same power balance at the algebraic level.

0.3. **Contributions**

The main contributions of this work are as follows. First, we derive a coupled field-line model in which a two-dimensional transverse electric Maxwell system interacts with a reduced transmission-line model through a distributed port. The coupling identifies the longitudinal voltage gradient along the line with the tangential electric field on the embedded curve and yields a formal power balance.
Second, we construct a closed operator realization of the coupled lossless interconnection on the physical energy space. The interior tangential trace is introduced as a closed operator, and the magnetic-field–cable block is defined through the adjoint of a minimal electric-field operator. For sufficiently regular states, this construction recovers the expected jump condition of the magnetic field across the embedded curve.
Third, the associated Green identity is used to obtain a boundary triplet that contains both the outer Maxwell port and a scalar cable port. This allows us to characterize conservative and dissipative boundary closures. In particular, maximally dissipative boundary relations lead to maximally dissipative realizations and hence to strongly continuous contraction semigroups.
Fourth, we develop a structure-preserving discretization based on the implicit midpoint rule and a compatible mixed finite element method. The electric field is approximated by lowest-order Nédélec elements, while the magnetic field and the line current are approximated by elementwise constants. If the embedded line is aligned with mesh edges, the coupling is represented directly by edge degrees of freedom. The fully discrete system preserves the port-Hamiltonian interconnection structure and satisfies an exact discrete power balance.
Finally, numerical experiments for a half-wave dipole antenna illustrate the coupled field-line dynamics and the energy behavior of the method.

0.4. **Organization**

In Section 1 we collect the functional-analytic notation, the dissipativity terminology, and the Sobolev trace setting used throughout the paper. Section 2 introduces the continuous Maxwell model, recalls the telegrapher equations, and derives the reduced current-field coupling together with the corresponding port-Hamiltonian power balance. In Section 3 we construct the closed operator realization and the associated boundary triplet. Section 4 uses this triplet to describe boundary closures and to prove semigroup generation for dissipative realizations. The structure-preserving time and space discretizations are developed in Section 5. Numerical experiments are presented in Section 6, and the paper concludes in Section 7.

1. Mathematical setting and notation

Technical trace and lifting results used in the proofs are collected in Appendix A.

1.1. **Functional-analytic conventions**

All spaces considered in this work are real. Accordingly, inner products and duality pairings are bilinear. For a normed space X, its continuous dual is denoted by X'. If X is a Hilbert space, the Riesz isomorphism $\mathcal{R}_X : X \to X'$ is characterized by $\langle \mathcal{R}_X x, \widetilde{x}\rangle_{X',X} = (x, \widetilde{x})_X$, $x, \widetilde{x} \in X$. Whenever an operator-theoretic result is stated in the literature for complex Hilbert spaces, it is applied to the complexification of the corresponding real operator. The resulting complex dynamics leave the real subspace invariant.
For normed spaces X and Y, we denote by $\mathcal{L}(X, Y)$ the space of bounded linear operators from X to Y. If $X = Y$, we write $\mathcal{L}(X) := \mathcal{L}(X, X)$. The identity on X is denoted by id_X. For a possibly unbounded operator A, the notation

$$A : \mathrm{dom}(A) \subset X \to Y$$

means that A is defined on the linear subspace $\mathrm{dom}(A)$ of X and takes values in Y. The symbols $\mathrm{dom}(A)$, $\ker(A)$, $\mathrm{ran}(A)$, and $\overline{A}$ denote its domain, kernel, range, and closure, respectively. If $D \subset \mathrm{dom}(A)$, then $A|_D$ denotes the restriction of A to the domain D. If X and Y are Hilbert spaces and A is densely defined, its

Hilbert-space adjoint is denoted by A^*. The *graph norm* of A is

$$\|x\|_{\mathrm{dom}(A)} := \big(\|x\|_X^2 + \|Ax\|_Y^2\big)^{1/2}.$$

If A is closed, then $\mathrm{dom}(A)$ equipped with this norm is a Hilbert space.
Duality pairings are written as $\langle\cdot,\cdot\rangle_{X',X}$, with the subscripts omitted when the spaces are clear from the context. If a Hilbert space is identified with its dual by the Riesz isomorphism, the corresponding duality pairing agrees with the Hilbert-space inner product. Owing to the extensive use of round brackets for inner products, square brackets are used for tuples and block vectors. Column vectors may be written in a single line with entries separated by semicolons.
For a Hilbert space X, a *linear relation* from X to X' is a linear subspace $\Theta \subset X \times X'$. It is called *closed* if it is closed in the product space $X \times X'$. It is called *dissipative* if $\langle f, e\rangle_{X',X} \le 0$ for all $(e,f) \in \Theta$. It is called *maximally dissipative* if it is dissipative and has no proper dissipative linear extension in $X \times X'$.
A linear operator $A : \mathrm{dom}(A) \subset X \to X$ on a Hilbert space X is viewed as a relation by identifying X with its dual via the Riesz isomorphism. Thus its graph is

$$\mathrm{gr}\, A := \{(x, \mathcal{R}_X Ax) : x \in \mathrm{dom}(A)\} \subset X \times X'.$$

The operator A is called *(maximally) dissipative* if this graph is (maximally) dissipative, as a relation. Consequently, A is dissipative if and only if $(Ax, x)_X \le 0$ for all $x \in \mathrm{dom}(A)$. For densely defined dissipative operators, maximal dissipativity is characterized by the Minty range condition

$$\mathrm{ran}(\lambda\,\mathrm{id}_X - A) = X$$

for some, and hence for every, $\lambda > 0$; see [15]. This is the form used in the Lumer–Phillips theorem for contractive semigroup generation. A densely defined operator A is called *skew-symmetric* if $(Ax, \widetilde{x})_X = -(x, A\widetilde{x})_X$ for all $x, \widetilde{x} \in \mathrm{dom}(A)$. If $A^* = -A$, then A is called *skew-adjoint*. We use the standard semigroup terminology, see [16]: a strongly continuous semigroup $(T(t))_{t\ge0}$ is *contractive* if $\|T(t)\|_{\mathcal{L}(X)} \le 1$ for all $t \ge 0$, and a strongly continuous group $(T(t))_{t\in\mathbb{R}}$ is *isometric* if each $T(t)$ is an isometry.

1.2. **Geometry, Sobolev spaces, and traces**

Throughout the paper, $\Omega \subset \mathbb{R}^2$ denotes a bounded Lipschitz domain. Its boundary is denoted by $\partial\Omega$, and $\boldsymbol{n} = (n_1, n_2)^\top$ is the outward unit normal on $\partial\Omega$. We use the associated unit tangent

$$\boldsymbol{\tau} := \left[\begin{smallmatrix} -n_2 \\ n_1 \end{smallmatrix}\right].$$

This convention fixes the signs in the Green identities used below.
The embedded transmission line is represented by an oriented curve $\Gamma \subset \Omega$ with $\overline{\Gamma} \subset \Omega$. More precisely, Γ is the relative interior of an embedded $C^{1,1}$ arc of length $\ell > 0$. Its closure is parametrized by an injective arc-length parametrization $\gamma : [0,\ell] \to \overline{\Gamma}$, and the orientation of Γ is induced by $\boldsymbol{\tau}_\Gamma(s) := \gamma'(s)$, $s \in [0,\ell]$. We set

$$\boldsymbol{n}_\Gamma(s) := \left[\begin{smallmatrix} -\tau_{\Gamma,2}(s) \\ \tau_{\Gamma,1}(s) \end{smallmatrix}\right].$$

We assume that γ admits an injective $C^{1,1}$ extension $\widetilde{\gamma} : (-\delta, \ell+\delta) \to \Omega$ for some $\delta > 0$ and that this extension has a tubular neighborhood. Thus there exist $\rho > 0$, an open set $U_\Gamma \subset \Omega$ with $\overline{U_\Gamma} \subset \Omega$, and a bi-Lipschitz map $\Psi : (-\delta, \ell+\delta) \times (-\rho, \rho) \longrightarrow U_\Gamma$ such that $\Psi(s,0) = \widetilde{\gamma}(s)$. The two sides of Γ are labeled by the signs of the transverse coordinate. If a scalar function q admits one-sided traces on Γ, its jump is denoted by

$$[\![q]\!]_\Gamma := \gamma_\Gamma^+ q - \gamma_\Gamma^- q.$$

The sign convention is the one induced by the above tubular coordinates.
In two space dimensions, the curl operator is understood according to the type of its argument. For a vector field $\boldsymbol{\phi} = (\phi_1, \phi_2)^\top$ and a scalar function q, we set

$$\nabla \times \boldsymbol{\phi} = \partial_1 \phi_2 - \partial_2 \phi_1, \qquad \nabla \times q = \begin{bmatrix} \partial_2 q \\ -\partial_1 q \end{bmatrix}.$$

The derivative with respect to the oriented arc-length variable along Γ is denoted by ∂_s, and $\mathbf{1}_\Gamma$ denotes the constant function with value one on Γ.
We denote by $(\cdot,\cdot)_\Omega$ and $\|\cdot\|_\Omega$ the $L^2(\Omega)$ inner product and norm. The corresponding quantities on Γ are denoted by $(\cdot,\cdot)_\Gamma$ and $\|\cdot\|_\Gamma$. The finite electric energy space is

$$H(\mathrm{curl}, \Omega) = \{\boldsymbol{\phi} \in L^2(\Omega)^2 : \nabla \times \boldsymbol{\phi} \in L^2(\Omega)\},$$

equipped with its natural graph norm. For functions on the embedded line we use

$$H^1(\Gamma) = \{q \in L^2(\Gamma) : \partial_s q \in L^2(\Gamma)\}.$$

For smooth fields, the outer tangential trace and scalar Dirichlet trace are

$$\gamma_\tau \boldsymbol{\phi} := \boldsymbol{\phi}|_{\partial\Omega} \cdot \boldsymbol{\tau}, \qquad \gamma_0 q := q|_{\partial\Omega}.$$

The Dirichlet trace extends to a bounded and surjective operator $\gamma_0 : H^1(\Omega) \to H^{1/2}(\partial\Omega)$ and admits a bounded right inverse; see [17, Thm. 3.38]. The tangential trace extends to a bounded operator

$$\gamma_\tau : H(\mathrm{curl}, \Omega) \to H^{-1/2}(\partial\Omega),$$

characterized by the Green identity

$$(\nabla \times \boldsymbol{\phi}, q)_\Omega - (\boldsymbol{\phi}, \nabla \times q)_\Omega = \langle \gamma_\tau \boldsymbol{\phi}, \gamma_0 q \rangle_{\partial\Omega}$$

for all $\boldsymbol{\phi} \in H(\mathrm{curl}, \Omega)$ and $q \in H^1(\Omega)$. We shall also use that γ_τ admits a bounded right inverse. The localization of such liftings away from compact subsets of Ω is stated separately in Lemma A.1.
The standard outer trace theory does not provide an $L^2(\Gamma)$ tangential restriction to the embedded curve. For smooth vector fields we therefore set

$$\gamma_\Gamma^\circ \boldsymbol{E} := (\boldsymbol{E}|_\Gamma) \cdot \boldsymbol{\tau}_\Gamma$$

and regard $\gamma_\Gamma^\circ : C^\infty(\overline{\Omega})^2 \subset H(\mathrm{curl}, \Omega) \to L^2(\Gamma)$ as a densely defined operator. This operator is closable; see Lemma A.2 in Appendix A. We denote its closure by γ_Γ and define

$$H_\Gamma(\mathrm{curl}, \Omega) := \mathrm{dom}(\gamma_\Gamma), \qquad \|\boldsymbol{E}\|^2_{H_\Gamma(\mathrm{curl},\Omega)} := \|\boldsymbol{E}\|^2_{H(\mathrm{curl},\Omega)} + \|\gamma_\Gamma \boldsymbol{E}\|^2_\Gamma.$$

Thus $H_\Gamma(\mathrm{curl}, \Omega)$ is a Hilbert space and $\gamma_\Gamma : H_\Gamma(\mathrm{curl}, \Omega) \to L^2(\Gamma)$ is bounded by construction. The outer tangential trace remains the standard bounded operator

$$\gamma_\tau : H_\Gamma(\mathrm{curl}, \Omega) \hookrightarrow H(\mathrm{curl}, \Omega) \longrightarrow H^{-1/2}(\partial\Omega).$$

In the proof of the boundary-map properties we use a cable lifting $\mathcal{L}_\Gamma : L^2(\Gamma) \to H_\Gamma(\mathrm{curl}, \Omega)$ constructed in Proposition A.3 in Appendix A.
Geometric trace setting. Throughout Sections 3 and 4 we assume that Ω and Γ satisfy the geometric hypotheses stated in Subsection 1.2. Moreover, γ_Γ denotes the closure of the interior tangential trace, and $H_\Gamma(\mathrm{curl}, \Omega) = \mathrm{dom}(\gamma_\Gamma)$ is equipped with the graph norm defined above. We also use the cable lifting from Proposition A.3 and the localized outer tangential trace lifting from Lemma A.1.

2. Continuous field-line model

In this section we derive the continuous field-line model used in the rest of the paper. We first recall the transverse-electric Maxwell system in the field domain and the telegrapher equations on the embedded line. We then impose the distributed port constraint that identifies the voltage gradient along the line with the tangential electric field. This yields a reduced current-field formulation whose formal power balance is made explicit. The closed operator realization is constructed later.

2.1. Maxwell's field equations

Let $T \in (0,\infty)$. The material parameters in the field domain are the permittivity ε, the permeability μ, and the conductivity σ. We assume

$$\varepsilon, \mu, \sigma \in L^\infty(\Omega), \qquad \varepsilon \geq \varepsilon_0 > 0, \qquad \mu \geq \mu_0 > 0, \qquad \sigma \geq 0$$

almost everywhere in Ω. In transverse-electric mode the electric field is represented by a two-dimensional vector field $\boldsymbol{E} = (E_x, E_y)^\top$, whereas the magnetic field is represented by a scalar field H_z. With an impressed current density $\boldsymbol{J}_0 \in L^2(0,T;L^2(\Omega)^2)$, Maxwell's curl equations reduce to

$$\varepsilon \dot{\boldsymbol{E}} = \nabla \times H_z - \sigma \boldsymbol{E} - \boldsymbol{J}_0, \qquad \mu \dot{H}_z = -\nabla \times \boldsymbol{E} \qquad \text{in } (0,T)\times\Omega.$$

Here $\nabla \times H_z$ denotes the vector-valued two-dimensional curl introduced in Subsection 1.2, and $\nabla \times \boldsymbol{E}$ denotes the scalar curl.
On the outer boundary we impose the Silver–Müller absorbing boundary condition

$$H_z - \eta E_\tau = 0 \qquad \text{on } (0,T)\times\partial\Omega, \tag{1}$$

where $E_\tau := \gamma_\tau \boldsymbol{E}$ and $\eta \in L^\infty(\partial\Omega)$ satisfies $\eta \geq 0$. For constant material parameters, the usual choice is $\eta = \sqrt{\varepsilon/\mu}$ on $\partial\Omega$.
At this stage the boundary condition is used only at the formal level. In particular, the boundary terms below are to be read for sufficiently regular fields, or after the boundary closure has been interpreted through the boundary variables introduced in Section 3. The same convention applies to the coupled weak formulation in Subsection 2.3.
The initial conditions are

$$\boldsymbol{E}(0) = \boldsymbol{E}^0, \qquad H_z(0) = H_z^0.$$

For sufficiently regular fields, the corresponding formal mixed formulation can be written on the test space

$$X_\Omega := H(\mathrm{curl},\Omega) \times L^2(\Omega).$$

It reads as follows. Find $[\boldsymbol{E}, H_z]$ such that, for almost every $t \in (0,T)$, the expressions below are well defined and

$$\begin{aligned} (\boldsymbol{\phi}, \varepsilon\dot{\boldsymbol{E}})_\Omega - (\nabla\times\boldsymbol{\phi}, H_z)_\Omega + (\boldsymbol{\phi}, \sigma\boldsymbol{E})_\Omega + \langle \eta\phi_\tau, E_\tau\rangle_{\partial\Omega} &= -(\boldsymbol{\phi}, \boldsymbol{J}_0)_\Omega, \\ (\psi, \mu\dot{H}_z)_\Omega + (\psi, \nabla\times\boldsymbol{E})_\Omega &= 0 \end{aligned} \tag{2}$$

for all $[\boldsymbol{\phi}, \psi] \in X_\Omega$. The boundary term in the first equation is the weak form of (1). The electromagnetic energy is

$$\mathcal{H}_\Omega(t) := \tfrac{1}{2}\|\sqrt{\varepsilon}\boldsymbol{E}(t)\|_\Omega^2 + \tfrac{1}{2}\|\sqrt{\mu}H_z(t)\|_\Omega^2.$$

Testing (2) with $[\boldsymbol{\phi}, \psi] = [\boldsymbol{E}, H_z]$ and adding the two equations gives the formal power balance

$$\tfrac{\mathrm{d}}{\mathrm{d}t}\mathcal{H}_\Omega + (\boldsymbol{E}, \sigma\boldsymbol{E})_\Omega + \langle \eta E_\tau, E_\tau\rangle_{\partial\Omega} = -(\boldsymbol{E}, \boldsymbol{J}_0)_\Omega.$$

Thus, conductivity in the field domain and the absorbing boundary condition contribute dissipative terms, while $\boldsymbol{J}_0$ represents an external power port.

2.2. **Telegrapher's line equations**

The embedded transmission line is described by its current I and potential V along Γ. The line parameters are the inductance L, capacitance C, resistance R, and conductance G per unit length. We assume

$$L, C, R, G \in L^\infty(\Gamma), \qquad L \geq L_0 > 0, \qquad C \geq C_0 > 0, \qquad R, G \geq 0$$

almost everywhere on Γ. The telegrapher equations are

$$L\dot{I} = -\partial_s V - RI, \qquad C\dot{V} = -\partial_s I - GV \qquad \text{in } (0,T)\times\Gamma.$$

We impose open-circuit boundary conditions

$$I(t,0) = I(t,\ell) = 0 \qquad \text{for } t \in (0,T), \tag{3}$$

and initial conditions

$$I(0) = I^0, \qquad V(0) = V^0.$$

The mixed weak formulation is posed on

$$X_\Gamma := L^2(\Gamma)\times H^1(\Gamma).$$

This weak formulation is to be understood as the formal energy identity associated with sufficiently regular line variables. A fully closed realization of the telegrapher system is not needed below, because the operator-theoretic part uses only the reduced current-field model introduced in the next subsection.
Find $[I,V]$ such that, for almost every $t \in (0,T)$, $[I(t),V(t)] \in X_\Gamma$ and

$$(p, L\dot{I})_\Gamma = -(p, \partial_s V)_\Gamma - (p, RI)_\Gamma, \quad (q, C\dot{V})_\Gamma = (\partial_s q, I)_\Gamma - (q, GV)_\Gamma \tag{4}$$

for all $[p,q] \in X_\Gamma$. The boundary condition (3) removes the endpoint contribution in the weak form of the second equation.
The line energy is

$$\mathcal{H}_\Gamma(t) := \tfrac{1}{2}\|\sqrt{L}I(t)\|_\Gamma^2 + \tfrac{1}{2}\|\sqrt{C}V(t)\|_\Gamma^2.$$

Testing (4) with $[p,q] = [I,V]$ gives

$$\tfrac{\mathrm{d}}{\mathrm{d}t}\mathcal{H}_\Gamma + (I, RI)_\Gamma + (V, GV)_\Gamma = 0.$$

The resistance and conductance therefore represent the internal dissipation mechanisms of the isolated line.

2.3. **Distributed port coupling**

The operator-theoretic realization below is based on a reduced current-field model. The full telegrapher system is used to motivate the port variables and, in particular, the relation between voltage gradient and tangential electric field. In the closed evolution system constructed in Sections 3 and 4, however, the retained cable state is the line current. Thus the capacitive voltage dynamics of the full telegrapher system is not part of the reduced realization analysed below. In particular, the reduced operator model does not impose endpoint traces of I at $s = 0, \ell$; instead, the remaining endpoint behavior is represented by the scalar cable port introduced in Section 3.
The field-line coupling is imposed through the compatibility condition that the tangential electric field along the embedded line equals the negative longitudinal voltage gradient,

$$\gamma_\Gamma \boldsymbol{E} = -\partial_s V \qquad \text{in } L^2(\Gamma). \tag{5}$$

Equivalently,

$$(p, \gamma_\Gamma \boldsymbol{E})_\Gamma = -(p, \partial_s V)_\Gamma \qquad \text{for all } p \in L^2(\Gamma).$$

Since $\gamma_\Gamma \boldsymbol{E}$ is required to belong to $L^2(\Gamma)$, the electric field is taken from the space $H_\Gamma(\mathrm{curl}, \Omega)$ introduced in Subsection 1.2.

In the coupled current-field formulation used below, the potential is eliminated from the first telegrapher equation by means of (5). Thus

$$L\dot{I} = \gamma_\Gamma \boldsymbol{E} - RI \qquad \text{on } \Gamma.$$

The reciprocal action of the line current on the electromagnetic field is represented by the weak term $-(\gamma_\Gamma \boldsymbol{\phi}, I)_\Gamma$ in the electric-field equation. This is the variational representation of a line-supported current source.

For sufficiently regular fields, the coupled formal weak formulation is written on the test space

$$Z := L^2(\Gamma) \times H_\Gamma(\mathrm{curl}, \Omega) \times L^2(\Omega).$$

It reads as follows. Find $[I, \boldsymbol{E}, H_z]$ such that, for almost every $t \in (0, T)$, the expressions below are well defined and

$$\begin{aligned} (p, L\dot{I})_\Gamma &= -(p, RI)_\Gamma + (p, \gamma_\Gamma \boldsymbol{E})_\Gamma, \\ (\boldsymbol{\phi}, \varepsilon \dot{\boldsymbol{E}})_\Omega &= -(\gamma_\Gamma \boldsymbol{\phi}, I)_\Gamma - (\boldsymbol{\phi}, \sigma \boldsymbol{E})_\Omega - \langle \eta \phi_\tau, E_\tau \rangle_{\partial\Omega} + (\nabla \times \boldsymbol{\phi}, H_z)_\Omega - (\boldsymbol{\phi}, \boldsymbol{J}_0)_\Omega, \\ (\psi, \mu \dot{H}_z)_\Omega &= -(\psi, \nabla \times \boldsymbol{E})_\Omega \end{aligned} \tag{6}$$

for all $[p, \boldsymbol{\phi}, \psi] \in Z$.

The term $(\gamma_\Gamma \boldsymbol{\phi}, I)_\Gamma$ is the weak action of the line-supported current. In strong distributional notation this corresponds to a singular current contribution supported on Γ. Accordingly, the scalar magnetic field may exhibit a jump across Γ while still belonging to $L^2(\Omega)$. The precise operator-theoretic treatment of this jump is deferred to Section 3.

The energy of the reduced coupled current-field system is

$$\mathcal{H}(t) := \tfrac{1}{2} \|\sqrt{L} I(t)\|_\Gamma^2 + \tfrac{1}{2} \|\sqrt{\varepsilon} \boldsymbol{E}(t)\|_\Omega^2 + \tfrac{1}{2} \|\sqrt{\mu} H_z(t)\|_\Omega^2.$$

Testing (6) with $[p, \boldsymbol{\phi}, \psi] = [I, \boldsymbol{E}, H_z]$ gives cancellation of the distributed interconnection terms and yields

$$\tfrac{\mathrm{d}}{\mathrm{d}t} \mathcal{H} + (I, RI)_\Gamma + (\boldsymbol{E}, \sigma \boldsymbol{E})_\Omega + \langle \eta E_\tau, E_\tau \rangle_{\partial\Omega} = -(\boldsymbol{E}, \boldsymbol{J}_0)_\Omega. \tag{7}$$

Thus, the field-line coupling is formally power-conserving, whereas the resistance, the conductivity, and the absorbing boundary condition are dissipative.

2.4. **Port-Hamiltonian structure and power balance**

The weak formulation (6) can be written in a compact port-Hamiltonian form. For

$$U = [I; \boldsymbol{E}; H_z] \in Z, \qquad W = [p; \boldsymbol{\phi}; \psi] \in Z,$$

define the mass form

$$M(W, U) := (p, LI)_\Gamma + (\boldsymbol{\phi}, \varepsilon \boldsymbol{E})_\Omega + (\psi, \mu H_z)_\Omega.$$

The interconnection form is

$$J(W, U) := (p, \gamma_\Gamma \boldsymbol{E})_\Gamma - (\gamma_\Gamma \boldsymbol{\phi}, I)_\Gamma + (\nabla \times \boldsymbol{\phi}, H_z)_\Omega - (\psi, \nabla \times \boldsymbol{E})_\Omega.$$

The dissipation form is

$$Q(W, U) := (p, RI)_\Gamma + (\boldsymbol{\phi}, \sigma \boldsymbol{E})_\Omega + \langle \eta \phi_\tau, E_\tau \rangle_{\partial\Omega},$$

and the external source functional is $B(W) := (\boldsymbol{\phi}, \boldsymbol{J}_0)_\Omega$. With these definitions, (6) is equivalently written as

$$M(W, \dot{U}) = J(W, U) - Q(W, U) - B(W) \qquad \text{for all } W \in Z. \tag{8}$$

The form M is symmetric and positive definite on the physical energy variables. Moreover, J is skew-symmetric, since

$$J(W, U) = -J(U, W) \qquad \text{for all } U, W \in Z,$$

and Q is symmetric and nonnegative. Hence, the Hamiltonian $\mathcal{H}(U) = \frac{1}{2}M(U, U)$ satisfies, at the formal level,

$$\tfrac{\mathrm{d}}{\mathrm{d}t}\mathcal{H}(U) + Q(U, U) = -B(U).$$

This is precisely the power balance (7). No well-posedness assertion is made at this stage; the purpose of the present section is only to identify the storage, interconnection, dissipation, and source terms of the continuous field-line model.

3. Operator-theoretic realization and boundary triplet

In this section, we construct a closed operator realization of the lossless field-line interconnection. The construction uses the interior tangential trace introduced in Subsection 1.2. The main point is that the electric field is coupled to an interior one-dimensional manifold, while the magnetic field may have a jump across this manifold.

In contrast to the ordering used in the weak formulation, we write the state in this section as

$$x = [I; H_z; \boldsymbol{E}].$$

This separates the magnetic-field–cable variables from the electric field and leads to an off-diagonal operator matrix.

3.1. **State spaces and operator blocks**

We set

$$\mathcal{X}_{\mathrm{mag}} := L^2(\Gamma) \times L^2(\Omega), \qquad \mathcal{X}_{\mathrm{el}} := L^2(\Omega)^2, \qquad \mathcal{X} := \mathcal{X}_{\mathrm{mag}} \times \mathcal{X}_{\mathrm{el}}.$$

Thus, for $x \in \mathcal{X}$ we write

$$x = [x_{\mathrm{mag}}; x_{\mathrm{el}}], \qquad x_{\mathrm{mag}} = [I; H_z], \qquad x_{\mathrm{el}} = \boldsymbol{E}.$$

All product spaces are equipped with their canonical Hilbert space structures.

The boundary variables take values in the mutually dual spaces

$$\mathcal{U} := H^{1/2}(\partial\Omega) \times \mathbb{R}, \qquad \mathcal{U}' := H^{-1/2}(\partial\Omega) \times \mathbb{R}.$$

Their duality pairing is

$$\left\langle \begin{bmatrix} f \\ y \end{bmatrix}, \begin{bmatrix} e \\ u \end{bmatrix} \right\rangle_{\mathcal{U}', \mathcal{U}} := \langle f, e \rangle_{\partial\Omega} + yu.$$

Here the first component describes the outer Maxwell port, while the second component describes the scalar cable port.

The lossless coupled operator will be realized as an off-diagonal matrix

$$\begin{bmatrix} 0 & \mathcal{A}_{\mathrm{el}} \\ \mathcal{A}_{\mathrm{mag}} & 0 \end{bmatrix}.$$

The electric-field block $\mathcal{A}_{\mathrm{el}}$ is defined directly. The magnetic-field–cable block $\mathcal{A}_{\mathrm{mag}}$ is then obtained as an adjoint operator. This avoids imposing a pointwise jump condition on H_z in the definition of the domain.

3.2. **The electric-field block**

Define

$$\mathcal{A}_{\mathrm{el}} : \mathrm{dom}(\mathcal{A}_{\mathrm{el}}) = H_\Gamma(\mathrm{curl}, \Omega) \longrightarrow \mathcal{X}_{\mathrm{mag}}, \quad \mathcal{A}_{\mathrm{el}} \boldsymbol{E} := \begin{bmatrix} \gamma_\Gamma \boldsymbol{E} \\ -\nabla \times \boldsymbol{E} \end{bmatrix}.$$

Since γ_Γ is closed as an operator from $H(\mathrm{curl}, \Omega)$ to $L^2(\Gamma)$, the operator $\mathcal{A}_{\mathrm{el}}$ is closed.
The associated electric boundary map is

$$\mathfrak{b}_{\mathrm{el}} : \mathrm{dom}(\mathcal{A}_{\mathrm{el}}) \longrightarrow \mathcal{U}', \qquad \mathfrak{b}_{\mathrm{el}} \boldsymbol{E} := \begin{bmatrix} -\gamma_\tau \boldsymbol{E} \\ \displaystyle\int_\Gamma \gamma_\Gamma \boldsymbol{E} \, \mathrm{d}s \end{bmatrix}.$$

It is bounded with respect to the graph norm of $\mathcal{A}_{\mathrm{el}}$.

Lemma 3.1. *Assume the geometric trace setting of Paragraph 1.2. Then the mapping $\mathfrak{b}_{\mathrm{el}} : \mathrm{dom}(\mathcal{A}_{\mathrm{el}}) \to \mathcal{U}'$ is surjective. Moreover,* $\ker \mathfrak{b}_{\mathrm{el}}$ *is dense in* $\mathcal{X}_{\mathrm{el}}$.

Proof. Let $[f; y] \in \mathcal{U}'$. By Lemma A.1, applied with $K = \overline{\Gamma}$, there exists $\boldsymbol{E}_f \in H(\mathrm{curl}, \Omega)$ such that $-\gamma_\tau \boldsymbol{E}_f = f$ and such that the support of $\boldsymbol{E}_f$ is separated from Γ. Since the support of $\boldsymbol{E}_f$ is separated from Γ, it can be approximated in $H(\mathrm{curl}, \Omega)$ by smooth fields whose supports are also separated from Γ. Hence $\boldsymbol{E}_f \in H_\Gamma(\mathrm{curl}, \Omega)$ and $\gamma_\Gamma \boldsymbol{E}_f = 0$. By Proposition A.3, $\boldsymbol{E}_y := \mathcal{L}_\Gamma((y/\ell)\mathbf{1}_\Gamma)$ satisfies

$$\gamma_\tau \boldsymbol{E}_y = 0, \qquad \int_\Gamma \gamma_\Gamma \boldsymbol{E}_y \, \mathrm{d}s = y.$$

Thus $\mathfrak{b}_{\mathrm{el}}(\boldsymbol{E}_f + \boldsymbol{E}_y) = [f; y]$.
Finally, $C_c^\infty(\Omega \setminus \Gamma)^2$ is contained in $\ker \mathfrak{b}_{\mathrm{el}}$ and is dense in $L^2(\Omega)^2$, since $\Gamma \cup \partial\Omega$ has two-dimensional Lebesgue measure zero. □

We define the minimal electric-field operator by

$$\mathring{\mathcal{A}}_{\mathrm{el}} := \mathcal{A}_{\mathrm{el}}\big|_{\ker \mathfrak{b}_{\mathrm{el}}}.$$

Since $\mathfrak{b}_{\mathrm{el}}$ is graph-norm continuous, $\mathring{\mathcal{A}}_{\mathrm{el}}$ is closed. By Lemma 3.1, it is also densely defined.

3.3. **The adjoint magnetic-field–cable block**

The magnetic-field–cable block is introduced through the adjoint of the minimal electric-field operator:

$$\mathcal{A}_{\mathrm{mag}} := -\mathring{\mathcal{A}}_{\mathrm{el}}^* : \mathrm{dom}(\mathcal{A}_{\mathrm{mag}}) \subset \mathcal{X}_{\mathrm{mag}} \longrightarrow \mathcal{X}_{\mathrm{el}}.$$

Thus, $\mathcal{A}_{\mathrm{mag}}$ is closed and densely defined.
For $z \in \mathrm{dom}(\mathcal{A}_{\mathrm{mag}})$ define

$$\Lambda_z(\boldsymbol{E}) := (\mathcal{A}_{\mathrm{el}} \boldsymbol{E}, z)_{\mathcal{X}_{\mathrm{mag}}} + (\boldsymbol{E}, \mathcal{A}_{\mathrm{mag}} z)_{\mathcal{X}_{\mathrm{el}}}, \qquad \boldsymbol{E} \in \mathrm{dom}(\mathcal{A}_{\mathrm{el}}).$$

By the definition of $\mathcal{A}_{\mathrm{mag}}$, this functional vanishes on $\ker \mathfrak{b}_{\mathrm{el}} = \mathrm{dom}(\mathring{\mathcal{A}}_{\mathrm{el}})$. Moreover, it is continuous with respect to the graph norm of $\mathcal{A}_{\mathrm{el}}$. Since $\mathfrak{b}_{\mathrm{el}} : \mathrm{dom}(\mathcal{A}_{\mathrm{el}}) \to \mathcal{U}'$ is bounded and surjective, Λ_z factors uniquely through $\mathfrak{b}_{\mathrm{el}}$. Hence there exists a unique $\mathfrak{b}_{\mathrm{mag}} z \in \mathcal{U}$ such that

$$(\mathcal{A}_{\mathrm{el}} \boldsymbol{E}, z)_{\mathcal{X}_{\mathrm{mag}}} + (\boldsymbol{E}, \mathcal{A}_{\mathrm{mag}} z)_{\mathcal{X}_{\mathrm{el}}} = \langle \mathfrak{b}_{\mathrm{el}} \boldsymbol{E}, \mathfrak{b}_{\mathrm{mag}} z \rangle_{\mathcal{U}', \mathcal{U}} \quad \text{for all } \boldsymbol{E} \in \mathrm{dom}(\mathcal{A}_{\mathrm{el}}). \tag{9}$$

The quotient mapping theorem also gives graph-norm boundedness of $\mathfrak{b}_{\mathrm{mag}}$. Indeed, there exists $c > 0$ such that, for all $z \in \mathrm{dom}(\mathcal{A}_{\mathrm{mag}})$,

$$\|\mathfrak{b}_{\mathrm{mag}} z\|_{\mathcal{U}} \le c\big(\|z\|_{\mathcal{X}_{\mathrm{mag}}} + \|\mathcal{A}_{\mathrm{mag}} z\|_{\mathcal{X}_{\mathrm{el}}}\big).$$

We also define the minimal magnetic-field–cable block by $\mathring{\mathcal{A}}_{\mathrm{mag}} := -\mathcal{A}_{\mathrm{el}}^*$. Then $\mathring{\mathcal{A}}_{\mathrm{mag}}$ is closed and densely defined, and $\mathring{\mathcal{A}}_{\mathrm{mag}} \subset \mathcal{A}_{\mathrm{mag}}$.

Lemma 3.2. *Assume the geometric trace setting of Paragraph 1.2. Then the mapping* $\mathfrak{b}_{\mathrm{mag}} : \mathrm{dom}(\mathcal{A}_{\mathrm{mag}}) \to \mathcal{U}$ *is surjective and* $\ker \mathfrak{b}_{\mathrm{mag}} = \mathrm{dom}(\mathring{\mathcal{A}}_{\mathrm{mag}})$.

Proof. First let $z \in \mathrm{dom}(\mathcal{A}_{\mathrm{mag}})$. By (9), $\mathfrak{b}_{\mathrm{mag}} z = 0$ if and only if

$$(\mathcal{A}_{\mathrm{el}} \boldsymbol{E}, z)_{\mathcal{X}_{\mathrm{mag}}} + (\boldsymbol{E}, \mathcal{A}_{\mathrm{mag}} z)_{\mathcal{X}_{\mathrm{el}}} = 0 \qquad \text{for all } \boldsymbol{E} \in \mathrm{dom}(\mathcal{A}_{\mathrm{el}}).$$

This is equivalent to $z \in \mathrm{dom}(\mathcal{A}_{\mathrm{el}}^*)$ and $\mathcal{A}_{\mathrm{el}}^* z = -\mathcal{A}_{\mathrm{mag}} z$, that is, $z \in \mathrm{dom}(\mathring{\mathcal{A}}_{\mathrm{mag}})$. This proves the kernel identity. It remains to prove surjectivity. Let $[e; u] \in \mathcal{U}$. Choose $H \in H^1(\Omega)$ with $\gamma_0 H = e$, and set $I := u \mathbf{1}_\Gamma$. Then $z := [I; H] \in \mathcal{X}_{\mathrm{mag}}$. For every $\boldsymbol{E} \in \mathrm{dom}(\mathcal{A}_{\mathrm{el}})$, the Green identity from Subsection 1.2 gives

$$-(\nabla \times \boldsymbol{E}, H)_\Omega + (\boldsymbol{E}, \nabla \times H)_\Omega = -\langle \gamma_\tau \boldsymbol{E}, e \rangle_{\partial\Omega}.$$

Thus

$$(\mathcal{A}_{\mathrm{el}} \boldsymbol{E}, z)_{\mathcal{X}_{\mathrm{mag}}} + (\boldsymbol{E}, \nabla \times H)_{\mathcal{X}_{\mathrm{el}}} = -\langle \gamma_\tau \boldsymbol{E}, e \rangle_{\partial\Omega} + u \int_\Gamma \gamma_\Gamma \boldsymbol{E} \, \mathrm{d}s.$$

For $\boldsymbol{E} \in \ker \mathfrak{b}_{\mathrm{el}}$ the right-hand side vanishes. Hence $z \in \mathrm{dom}(\mathcal{A}_{\mathrm{mag}})$ and $\mathcal{A}_{\mathrm{mag}} z = \nabla \times H$. Comparing the last identity with (9) yields $\mathfrak{b}_{\mathrm{mag}} z = [e; u]$. Therefore $\mathfrak{b}_{\mathrm{mag}}$ is surjective. □

3.4. **Classical interpretation**

The abstract magnetic-field–cable block has the expected interpretation for sufficiently regular states. Suppose that H_z is H^1 on both sides of Γ, possesses an outer trace $\gamma_0 H_z \in H^{1/2}(\partial\Omega)$, and admits one-sided traces on Γ. With the sign convention introduced in Subsection 1.2, the slit-domain Green identity reads

$$(\nabla \times \boldsymbol{E}, H_z)_\Omega - (\boldsymbol{E}, \nabla \times H_z)_\Omega = \langle \gamma_\tau \boldsymbol{E}, \gamma_0 H_z \rangle_{\partial\Omega} - (\gamma_\Gamma \boldsymbol{E}, [\![H_z]\!]_\Gamma)_\Gamma.$$

Initially valid for smooth fields on the slit domain, this identity extends to $\boldsymbol{E} \in \mathrm{dom}(\mathcal{A}_{\mathrm{el}})$ by the definition of the closed interior trace and by density in the graph norm.

Proposition 3.3. *Assume the geometric trace setting of Paragraph 1.2. Let* $I \in L^2(\Gamma)$. *Let* $H_z \in L^2(\Omega)$ *be such that its restrictions to the two sides of the slit domain* $\Omega \setminus \overline{\Gamma}$ *have* H^1_{loc}*-regularity up to* Γ, *that its piecewise curl belongs to* $L^2(\Omega)^2$, *that* $\gamma_0 H_z \in H^{1/2}(\partial\Omega)$, *and that the one-sided traces on* Γ *exist with* $[\![H_z]\!]_\Gamma \in L^2(\Gamma)$. *Then* $[I; H_z] \in \mathrm{dom}(\mathcal{A}_{\mathrm{mag}})$ *if and only if there exists* $i_{\mathrm{c}} \in \mathbb{R}$ *such that*

$$[\![H_z]\!]_\Gamma + I = i_{\mathrm{c}} \mathbf{1}_\Gamma.$$

In this case,

$$\mathcal{A}_{\mathrm{mag}} \begin{bmatrix} I \\ H_z \end{bmatrix} = \nabla \times H_z, \qquad \mathfrak{b}_{\mathrm{mag}} \begin{bmatrix} I \\ H_z \end{bmatrix} = \begin{bmatrix} \gamma_0 H_z \\ i_{\mathrm{c}} \end{bmatrix},$$

where the curl is taken separately on the two sides of Γ.

Proof. Set $z = [I; H_z]$.
Assume first that $[\![H_z]\!]_\Gamma + I = i_{\mathrm{c}} \mathbf{1}_\Gamma$. For every $\boldsymbol{E} \in \mathrm{dom}(\mathring{\mathcal{A}}_{\mathrm{el}})$ we have $\gamma_\tau \boldsymbol{E} = 0$ and $\int_\Gamma \gamma_\Gamma \boldsymbol{E} \, \mathrm{d}s = 0$. The slit-domain Green identity therefore gives

$$(\mathring{\mathcal{A}}_{\mathrm{el}} \boldsymbol{E}, z)_{\mathcal{X}_{\mathrm{mag}}} = -(\boldsymbol{E}, \nabla \times H_z)_{\mathcal{X}_{\mathrm{el}}}.$$

Hence $z \in \mathrm{dom}(\mathring{\mathcal{A}}_{\mathrm{el}}^*)$ and $\mathring{\mathcal{A}}_{\mathrm{el}}^* z = -\nabla \times H_z$. By the definition of $\mathcal{A}_{\mathrm{mag}}$, this means that $z \in \mathrm{dom}(\mathcal{A}_{\mathrm{mag}})$ and $\mathcal{A}_{\mathrm{mag}} z = \nabla \times H_z$.
For arbitrary $\boldsymbol{E} \in \mathrm{dom}(\mathcal{A}_{\mathrm{el}})$, the same Green identity gives

$$(\mathcal{A}_{\mathrm{el}}\boldsymbol{E}, z)_{\mathcal{X}_{\mathrm{mag}}} + (\boldsymbol{E}, \mathcal{A}_{\mathrm{mag}} z)_{\mathcal{X}_{\mathrm{el}}} = -\langle \gamma_\tau \boldsymbol{E}, \gamma_0 H_z \rangle_{\partial\Omega} + i_{\mathrm{c}} \int_\Gamma \gamma_\Gamma \boldsymbol{E} \,\mathrm{d}s.$$

Comparison with (9) yields

$$\mathfrak{b}_{\mathrm{mag}} z = \begin{bmatrix} \gamma_0 H_z \\ i_{\mathrm{c}} \end{bmatrix}.$$

Conversely, assume that $z = [I; H_z] \in \mathrm{dom}(\mathcal{A}_{\mathrm{mag}})$ and write $\mathfrak{b}_{\mathrm{mag}} z = [e; u]$. Comparing (9) with the slit-domain Green identity gives

$$-\langle \gamma_\tau \boldsymbol{E}, e \rangle_{\partial\Omega} + u \int_\Gamma \gamma_\Gamma \boldsymbol{E} \,\mathrm{d}s = -\langle \gamma_\tau \boldsymbol{E}, \gamma_0 H_z \rangle_{\partial\Omega} + (\gamma_\Gamma \boldsymbol{E}, [\![H_z]\!]_\Gamma + I)_\Gamma$$

for all $\boldsymbol{E} \in \mathrm{dom}(\mathcal{A}_{\mathrm{el}})$.
Choose $\boldsymbol{E} = \mathcal{L}_\Gamma g$ with arbitrary $g \in L^2(\Gamma)$. Since $\gamma_\tau \mathcal{L}_\Gamma g = 0$ and $\gamma_\Gamma \mathcal{L}_\Gamma g = g$, we obtain

$$(g, [\![H_z]\!]_\Gamma + I)_\Gamma = u \int_\Gamma g \,\mathrm{d}s \qquad \text{for all } g \in L^2(\Gamma).$$

Thus $[\![H_z]\!]_\Gamma + I = u \mathbf{1}_\Gamma$.
Finally, choosing outer tangential-trace liftings with support separated from Γ gives $e = \gamma_0 H_z$. Hence $u = i_{\mathrm{c}}$ and the asserted formula for $\mathfrak{b}_{\mathrm{mag}} z$ follows. □

For regular states the second component i_{c} of $\mathfrak{b}_{\mathrm{mag}}[I; H_z]$ is therefore the terminal current associated with the constant part of the total jump-current balance $[\![H_z]\!]_\Gamma + I$. The conjugate terminal voltage is

$$v_{\mathrm{c}} = \int_\Gamma \gamma_\Gamma \boldsymbol{E} \,\mathrm{d}s,$$

which is the voltage drop induced by the tangential electric field along the embedded line.

3.5. **Minimal and maximal realizations**

We now combine the two off-diagonal blocks. Define

$$\mathcal{J}_{\min} := \begin{bmatrix} 0 & \mathring{\mathcal{A}}_{\mathrm{el}} \\ \mathring{\mathcal{A}}_{\mathrm{mag}} & 0 \end{bmatrix}, \qquad \mathrm{dom}(\mathcal{J}_{\min}) = \mathrm{dom}(\mathring{\mathcal{A}}_{\mathrm{mag}}) \times \mathrm{dom}(\mathring{\mathcal{A}}_{\mathrm{el}}),$$
$$\mathcal{J}_{\max} := \begin{bmatrix} 0 & \mathcal{A}_{\mathrm{el}} \\ \mathcal{A}_{\mathrm{mag}} & 0 \end{bmatrix}, \qquad \mathrm{dom}(\mathcal{J}_{\max}) = \mathrm{dom}(\mathcal{A}_{\mathrm{mag}}) \times \mathrm{dom}(\mathcal{A}_{\mathrm{el}}).$$

Thus, for $x = [I; H_z; \boldsymbol{E}] \in \mathrm{dom}(\mathcal{J}_{\max})$,

$$\mathcal{J}_{\max} x = \begin{bmatrix} \gamma_\Gamma \boldsymbol{E} \\ -\nabla \times \boldsymbol{E} \\ \mathcal{A}_{\mathrm{mag}}[I; H_z] \end{bmatrix}.$$

For regular states satisfying the jump condition from Proposition 3.3, the last component is the piecewise curl of H_z.

The adjoint relations of the off-diagonal blocks imply

$$\mathcal{J}_{\max} = -\mathcal{J}_{\min}^*, \qquad \mathcal{J}_{\min} = -\mathcal{J}_{\max}^*.$$

Consequently, $\mathcal{J}_{\min}$ is closed, densely defined, and skew-symmetric. The operator $\mathcal{J}_{\max}$ is the corresponding maximal adjoint realization.
For $x = [I; H_z; \boldsymbol{E}] \in \operatorname{dom}(\mathcal{J}_{\max})$, define

$$\mathfrak{B}_1 x := \mathfrak{b}_{\mathrm{mag}} \begin{bmatrix} I \\ H_z \end{bmatrix} \in \mathcal{U}, \qquad \mathfrak{B}_2 x := \mathfrak{b}_{\mathrm{el}} \boldsymbol{E} \in \mathcal{U}'.$$

For regular states, this means

$$\mathfrak{B}_1 x = \begin{bmatrix} \gamma_0 H_z \\ i_{\mathrm{c}} \end{bmatrix}, \qquad \mathfrak{B}_2 x = \begin{bmatrix} -\gamma_\tau \boldsymbol{E} \\ v_{\mathrm{c}} \end{bmatrix}, \qquad v_{\mathrm{c}} = \int_\Gamma \gamma_\Gamma \boldsymbol{E} \, \mathrm{d}s.$$

Combining (9) for two states yields the abstract Green identity

$$(\mathcal{J}_{\max} x, \widetilde{x})_{\mathcal{X}} + (x, \mathcal{J}_{\max} \widetilde{x})_{\mathcal{X}} = \langle \mathfrak{B}_2 x, \mathfrak{B}_1 \widetilde{x} \rangle_{\mathcal{U}',\mathcal{U}} + \langle \mathfrak{B}_2 \widetilde{x}, \mathfrak{B}_1 x \rangle_{\mathcal{U}',\mathcal{U}}$$
$$\text{for all } x, \widetilde{x} \in \operatorname{dom}(\mathcal{J}_{\max}). \quad (10)$$

Proposition 3.4. *Assume the geometric trace setting of Paragraph 1.2, and let $\mathcal{J}_{\min}$, $\mathcal{J}_{\max}$, $\mathfrak{B}_1$, and $\mathfrak{B}_2$ be the operators and boundary maps defined above. Then $\mathfrak{B}_1$ and $\mathfrak{B}_2$ are bounded with respect to the graph norm of $\mathcal{J}_{\max}$. Moreover, the combined mapping*

$$\begin{bmatrix} \mathfrak{B}_1 \\ \mathfrak{B}_2 \end{bmatrix} : \operatorname{dom}(\mathcal{J}_{\max}) \longrightarrow \mathcal{U} \times \mathcal{U}'$$

is surjective, and

$$\operatorname{dom}(\mathcal{J}_{\min}) = \ker \mathfrak{B}_1 \cap \ker \mathfrak{B}_2.$$

Proof. Graph-norm boundedness follows from the graph-norm boundedness of $\mathfrak{b}_{\mathrm{mag}}$ and $\mathfrak{b}_{\mathrm{el}}$.
Since the magnetic-field–cable variable and the electric variable can be chosen independently, the surjectivity of the combined boundary mapping is a consequence of Lemma 3.2 and Lemma 3.1.
It remains to identify the kernel of the combined boundary map. Since $\mathfrak{B}_1$ acts only on the magnetic-field–cable component and $\mathfrak{B}_2$ acts only on the electric component, we have

$$\ker \mathfrak{B}_1 \cap \ker \mathfrak{B}_2 = \ker \mathfrak{b}_{\mathrm{mag}} \times \ker \mathfrak{b}_{\mathrm{el}}.$$

Using Lemma 3.2 and the definition of $\mathring{\mathcal{A}}_{\mathrm{el}}$, this becomes

$$\ker \mathfrak{B}_1 \cap \ker \mathfrak{B}_2 = \operatorname{dom}(\mathring{\mathcal{A}}_{\mathrm{mag}}) \times \operatorname{dom}(\mathring{\mathcal{A}}_{\mathrm{el}}) = \operatorname{dom}(\mathcal{J}_{\min}).$$

□

For regular states, the condition $x \in \operatorname{dom}(\mathcal{J}_{\min})$ amounts to

$$\gamma_\tau \boldsymbol{E} = 0, \qquad \int_\Gamma \gamma_\Gamma \boldsymbol{E} \, \mathrm{d}s = 0, \qquad \gamma_0 H_z = 0, \qquad [\![H_z]\!]_\Gamma + I = 0.$$

Thus, the minimal realization closes both the outer Maxwell port and the scalar cable port.

3.6. **Boundary-triplet formulation**

We now put the preceding Green identity into the standard boundary-triplet form for skew-symmetric operators. Let $\mathcal{R}_{\mathcal{U}} : \mathcal{U} \to \mathcal{U}'$ denote the Riesz isomorphism, that is,

$$\langle \mathcal{R}_{\mathcal{U}} e, \widetilde{e} \rangle_{\mathcal{U}',\mathcal{U}} = (e, \widetilde{e})_{\mathcal{U}} \quad \text{for all } e, \widetilde{e} \in \mathcal{U}.$$

The dual-space boundary variable $\mathfrak{B}_2 x \in \mathcal{U}'$ is then converted into an element of $\mathcal{U}$ by $\mathcal{R}_{\mathcal{U}}^{-1}\mathfrak{B}_2 x$.
Let S be a closed, densely defined, skew-symmetric operator on a Hilbert space X, and set $S_{\max} := -S^*$. A triple (E, Γ_1, Γ_2) is called a *boundary triplet* for S if $\Gamma_1, \Gamma_2 : \operatorname{dom}(S_{\max}) \to E$ are graph-norm continuous, the map $[\Gamma_1; \Gamma_2] : \operatorname{dom}(S_{\max}) \to E \times E$ is surjective,

$$(S_{\max} x, \widetilde{x})_X + (x, S_{\max} \widetilde{x})_X = (\Gamma_2 x, \Gamma_1 \widetilde{x})_E + (\Gamma_2 \widetilde{x}, \Gamma_1 x)_E$$

for all $x, \widetilde{x} \in \operatorname{dom}(S_{\max})$, and $\operatorname{dom}(S) = \ker \Gamma_1 \cap \ker \Gamma_2$. We use the same terminology for the dual-pair formulation if the second boundary variable takes values in E' and becomes an ordinary boundary triplet after applying the Riesz isomorphism.

Theorem 3.5. *Assume the geometric trace setting of Paragraph 1.2. Let $\mathcal{J}_{\min}$, $\mathcal{J}_{\max}$, $\mathfrak{B}_1$, and $\mathfrak{B}_2$ be the operators and boundary maps defined in Subsection 3.5. Then $\mathcal{J}_{\min}$ is closed, densely defined, and skew-symmetric, $\mathcal{J}_{\max} = -\mathcal{J}_{\min}^*$, and*

$$\big(\mathcal{U}, \mathfrak{B}_1, \mathcal{R}_{\mathcal{U}}^{-1}\mathfrak{B}_2\big)$$

is a boundary triplet for $\mathcal{J}_{\min}$. Equivalently, $(\mathfrak{B}_1, \mathfrak{B}_2)$ is a boundary triplet over the dual pair $(\mathcal{U}, \mathcal{U}')$.

Proof. The adjoint identities and the basic properties of $\mathcal{J}_{\min}$ were established in Subsection 3.5. In particular, $\mathcal{J}_{\min}$ is closed, densely defined, and skew-symmetric, and $\mathcal{J}_{\max} = -\mathcal{J}_{\min}^*$. The Green identity is precisely (10). After applying the Riesz isomorphism to the second boundary variable, this identity takes the standard boundary-triplet form. The graph-norm boundedness, surjectivity, and kernel condition required in the definition follow from Proposition 3.4. □

Consequently, closed extensions of $\mathcal{J}_{\min}$ contained in $\mathcal{J}_{\max}$ are obtained by imposing closed linear relations between $\mathfrak{B}_1 x$ and $\mathfrak{B}_2 x$. This is the starting point for the dissipative and conservative boundary closures in Section 4.

Remark 3.6. The construction extends to a finite family of pairwise disjoint embedded cables $\Gamma = \dot{\bigcup}_{j=1}^{m} \Gamma_j$. Each cable contributes one scalar cable port. The boundary spaces are then

$$\mathcal{U} = H^{1/2}(\partial\Omega) \times \mathbb{R}^m, \qquad \mathcal{U}' = H^{-1/2}(\partial\Omega) \times \mathbb{R}^m,$$

and the preceding construction applies componentwise. ◇

4. Boundary closures and semigroup generation

We now use the boundary triplet from Theorem 3.5 to define autonomous realizations of the coupled field-line operator. The boundary variables are $\mathfrak{B}_1 x \in \mathcal{U}$ and $\mathfrak{B}_2 x \in \mathcal{U}'$, and the corresponding boundary power is $\langle \mathfrak{B}_2 x, \mathfrak{B}_1 x \rangle_{\mathcal{U}',\mathcal{U}}$. Dissipative boundary closures are therefore described by dissipative linear relations between these two variables. After the boundary closure has been fixed, the material coefficients and the internal damping are incorporated through the physical energy inner product.

4.1. **Autonomous boundary closures**

Let $\Theta \subset \mathcal{U} \times \mathcal{U}'$ be a linear relation. The corresponding realization of $\mathcal{J}_{\max}$ is defined by

$$\operatorname{dom}(\mathcal{J}_\Theta) := \{x \in \operatorname{dom}(\mathcal{J}_{\max}) : (\mathfrak{B}_1 x, \mathfrak{B}_2 x) \in \Theta\}, \qquad \mathcal{J}_\Theta x := \mathcal{J}_{\max} x.$$

Thus $\mathcal{J}_{\min} \subset \mathcal{J}_\Theta \subset \mathcal{J}_{\max}$. Since the combined boundary mapping is continuous with respect to the graph norm of $\mathcal{J}_{\max}$, the operator $\mathcal{J}_\Theta$ is closed whenever Θ is closed. Dissipativity and maximal dissipativity of Θ are understood in the sense of Subsection 1.1. For a linear relation $\Theta \subset \mathcal{U} \times \mathcal{U}'$, define its *power-orthogonal relation* by

$$\Theta^{[\perp]} := \left\{(e, f) \in \mathcal{U} \times \mathcal{U}' : \langle f, \widetilde{e}\rangle_{\mathcal{U}',\mathcal{U}} + \langle \widetilde{f}, e\rangle_{\mathcal{U}',\mathcal{U}} = 0 \text{ for all } (\widetilde{e}, \widetilde{f}) \in \Theta\right\}.$$

A relation satisfying $\Theta = \Theta^{[\perp]}$ is called *maximally power-conserving.*

Theorem 4.1. *Assume the geometric trace setting of Paragraph 1.2, and let $\Theta \subset \mathcal{U} \times \mathcal{U}'$ be a closed linear relation. Define $\mathcal{J}_\Theta$ by*

$$\operatorname{dom}(\mathcal{J}_\Theta) = \{x \in \operatorname{dom}(\mathcal{J}_{\max}) : (\mathfrak{B}_1 x, \mathfrak{B}_2 x) \in \Theta\}, \qquad \mathcal{J}_\Theta x = \mathcal{J}_{\max} x.$$

Then the following statements hold.

1. *$\mathcal{J}_\Theta$ is dissipative on $\mathcal{X}$ if and only if Θ is dissipative.*
2. *$\mathcal{J}_\Theta$ is maximally dissipative on $\mathcal{X}$ if and only if Θ is maximally dissipative.*
3. *The adjoint realization satisfies $-\mathcal{J}_\Theta^* = \mathcal{J}_{\Theta^{[\perp]}}$. In particular, $\mathcal{J}_\Theta$ is skew-adjoint if and only if Θ is maximally power-conserving.*

Proof. We first reduce the dual-pair formulation to the standard Hilbert-space form of a boundary triplet. Let

$$\widehat{\Theta} := \{(e, g) \in \mathcal{U} \times \mathcal{U} : (e, \mathcal{R}_{\mathcal{U}} g) \in \Theta\}.$$

Thus $\widehat{\Theta}$ is the image of Θ under the identification of $\mathcal{U}'$ with $\mathcal{U}$ by the Riesz isomorphism. In particular,

$$(\mathfrak{B}_1 x, \mathfrak{B}_2 x) \in \Theta \quad \Longleftrightarrow \quad (\mathfrak{B}_1 x, \mathcal{R}_{\mathcal{U}}^{-1} \mathfrak{B}_2 x) \in \widehat{\Theta}.$$

Hence $\mathcal{J}_\Theta$ is precisely the extension of $\mathcal{J}_{\min}$ determined by the boundary relation $\widehat{\Theta}$ for the ordinary boundary triplet $\left(\mathcal{U}, \mathfrak{B}_1, \mathcal{R}_{\mathcal{U}}^{-1}\mathfrak{B}_2\right)$ from Theorem 3.5. This is the relation-valued version of the standard boundary-triplet extension theorem; see, e.g., [18, Prop. 2.2]. The operator-valued skew-symmetric formulation is given in [19, Thm. 4.2 and Prop. 4.8]. Moreover, $\langle f, e\rangle_{\mathcal{U}',\mathcal{U}} = (\mathcal{R}_{\mathcal{U}}^{-1} f, e)_{\mathcal{U}}$, so Θ is dissipative in the dual-pair sense if and only if $\widehat{\Theta}$ is dissipative as a relation in the Hilbert space $\mathcal{U}$.
For $x \in \operatorname{dom}(\mathcal{J}_\Theta)$, the Green identity (10) with $\widetilde{x} = x$ gives

$$(\mathcal{J}_\Theta x, x)_{\mathcal{X}} = \langle \mathfrak{B}_2 x, \mathfrak{B}_1 x\rangle_{\mathcal{U}',\mathcal{U}}.$$

If Θ is dissipative, then the right-hand side is nonpositive for all $x \in \operatorname{dom}(\mathcal{J}_\Theta)$, and hence $\mathcal{J}_\Theta$ is dissipative.
Conversely, assume that $\mathcal{J}_\Theta$ is dissipative and let $(e, f) \in \Theta$. By the surjectivity of the combined boundary mapping from Proposition 3.4, there exists $x \in \operatorname{dom}(\mathcal{J}_{\max})$ such that $\mathfrak{B}_1 x = e$, $\mathfrak{B}_2 x = f$. Then $x \in \operatorname{dom}(\mathcal{J}_\Theta)$, and therefore $\langle f, e\rangle_{\mathcal{U}',\mathcal{U}} = (\mathcal{J}_\Theta x, x)_{\mathcal{X}} \le 0$. Thus Θ is dissipative. This proves (1).
We next prove maximal dissipativity. Assume first that Θ is maximally dissipative. Let $\mathcal{K}$ be a dissipative extension of $\mathcal{J}_\Theta$. Since $\mathcal{J}_{\min} \subset \mathcal{J}_\Theta \subset \mathcal{K}$ and $\mathcal{J}_{\min}$ is skew-symmetric, every dissipative extension of $\mathcal{J}_{\min}$ is contained in $-\mathcal{J}_{\min}^* = \mathcal{J}_{\max}$. Hence $\mathcal{K} \subset \mathcal{J}_{\max}$. Define the boundary relation

$$\Theta_{\mathcal{K}} := \{(\mathfrak{B}_1 x, \mathfrak{B}_2 x) : x \in \operatorname{dom}(\mathcal{K})\} \subset \mathcal{U} \times \mathcal{U}'.$$

For $x \in \operatorname{dom}(\mathcal{K})$ the Green identity with $\widetilde{x} = x$ yields $\langle \mathfrak{B}_2 x, \mathfrak{B}_1 x\rangle_{\mathcal{U}',\mathcal{U}} = (\mathcal{K}x, x)_{\mathcal{X}} \le 0$. Thus $\Theta_{\mathcal{K}}$ is dissipative. Since $\mathcal{K}$ extends $\mathcal{J}_\Theta$, we have $\Theta \subset \Theta_{\mathcal{K}}$. By maximal dissipativity of Θ, it follows that $\Theta_{\mathcal{K}} = \Theta$. Hence every $x \in \operatorname{dom}(\mathcal{K})$ satisfies $(\mathfrak{B}_1 x, \mathfrak{B}_2 x) \in \Theta$, and therefore $x \in \operatorname{dom}(\mathcal{J}_\Theta)$. Thus $\mathcal{K} = \mathcal{J}_\Theta$, and $\mathcal{J}_\Theta$ is maximally dissipative.

Conversely, assume that $\mathcal{J}_\Theta$ is maximally dissipative. Let $\widetilde{\Theta}$ be a dissipative linear relation with $\Theta \subset \widetilde{\Theta}$. Then the corresponding realization $\mathcal{J}_{\widetilde{\Theta}}$ is dissipative by part (1), and it is a dissipative extension of $\mathcal{J}_\Theta$. Hence maximal dissipativity of $\mathcal{J}_\Theta$ gives $\mathcal{J}_{\widetilde{\Theta}} = \mathcal{J}_\Theta$. Let $(e, f) \in \widetilde{\Theta}$. Again by the surjectivity of the combined boundary mapping, choose $x \in \operatorname{dom}(\mathcal{J}_{\max})$ with $\mathfrak{B}_1 x = e$, $\mathfrak{B}_2 x = f$. Then $x \in \operatorname{dom}(\mathcal{J}_{\widetilde{\Theta}}) = \operatorname{dom}(\mathcal{J}_\Theta)$, and hence $(e, f) \in \Theta$. Therefore $\widetilde{\Theta} = \Theta$, and Θ is maximally dissipative. This proves (2).

It remains to identify the adjoint realization. Let $y \in \operatorname{dom}(\mathcal{J}_{\Theta^{[\perp]}})$. Then $y \in \operatorname{dom}(\mathcal{J}_{\max})$ and $(\mathfrak{B}_1 y, \mathfrak{B}_2 y) \in \Theta^{[\perp]}$. For every $x \in \operatorname{dom}(\mathcal{J}_\Theta)$ we have $(\mathfrak{B}_1 x, \mathfrak{B}_2 x) \in \Theta$, and therefore $\langle \mathfrak{B}_2 y, \mathfrak{B}_1 x\rangle_{\mathcal{U}',\mathcal{U}} + \langle \mathfrak{B}_2 x, \mathfrak{B}_1 y\rangle_{\mathcal{U}',\mathcal{U}} = 0$. Using the Green identity, we obtain

$$(\mathcal{J}_\Theta x, y)_{\mathcal{X}} + (x, \mathcal{J}_{\max} y)_{\mathcal{X}} = 0 \qquad \text{for all } x \in \operatorname{dom}(\mathcal{J}_\Theta).$$

Hence $y \in \operatorname{dom}(\mathcal{J}_\Theta^*)$ and $\mathcal{J}_\Theta^* y = -\mathcal{J}_{\max} y$, that is, $y \in \operatorname{dom}(-\mathcal{J}_\Theta^*)$ and $-\mathcal{J}_\Theta^* y = \mathcal{J}_{\max} y = \mathcal{J}_{\Theta^{[\perp]}} y$. Thus $\mathcal{J}_{\Theta^{[\perp]}} \subset -\mathcal{J}_\Theta^*$.

Conversely, let $y \in \operatorname{dom}(\mathcal{J}_\Theta^*)$. Since $\mathcal{J}_{\min} \subset \mathcal{J}_\Theta$, we have $\mathcal{J}_\Theta^* \subset \mathcal{J}_{\min}^* = -\mathcal{J}_{\max}$. Consequently, $y \in \operatorname{dom}(\mathcal{J}_{\max})$ and $\mathcal{J}_\Theta^* y = -\mathcal{J}_{\max} y$. Hence, $(\mathcal{J}_\Theta x, y)_{\mathcal{X}} + (x, \mathcal{J}_{\max} y)_{\mathcal{X}} = 0$ for all $x \in \operatorname{dom}(\mathcal{J}_\Theta)$. By the Green identity this is equivalent to

$$\langle \mathfrak{B}_2 y, \mathfrak{B}_1 x\rangle_{\mathcal{U}',\mathcal{U}} + \langle \mathfrak{B}_2 x, \mathfrak{B}_1 y\rangle_{\mathcal{U}',\mathcal{U}} = 0 \qquad \text{for all } x \in \operatorname{dom}(\mathcal{J}_\Theta).$$

Since the combined boundary mapping is surjective, the boundary values of elements of $\operatorname{dom}(\mathcal{J}_\Theta)$ are exactly the elements of Θ. Therefore $(\mathfrak{B}_1 y, \mathfrak{B}_2 y) \in \Theta^{[\perp]}$. Thus $y \in \operatorname{dom}(\mathcal{J}_{\Theta^{[\perp]}})$ and $-\mathcal{J}_\Theta^* y = \mathcal{J}_{\Theta^{[\perp]}} y$. We have proved $-\mathcal{J}_\Theta^* = \mathcal{J}_{\Theta^{[\perp]}}$.

Finally, $\mathcal{J}_\Theta$ is skew-adjoint if and only if $\mathcal{J}_\Theta = -\mathcal{J}_\Theta^*$. By the adjoint formula just proved, this is equivalent to $\mathcal{J}_\Theta = \mathcal{J}_{\Theta^{[\perp]}}$. Using the surjectivity of the boundary map once more, equality of these realizations is equivalent to $\Theta = \Theta^{[\perp]}$. Thus $\mathcal{J}_\Theta$ is skew-adjoint if and only if Θ is maximally power-conserving. This proves (3). □

4.2. **Relevant boundary configurations**

For regular states we write

$$\mathfrak{B}_1 x = \begin{bmatrix} e_{\mathrm{M}} \\ i_{\mathrm{c}} \end{bmatrix}, \qquad \mathfrak{B}_2 x = \begin{bmatrix} f_{\mathrm{M}} \\ v_{\mathrm{c}} \end{bmatrix},$$

where $e_{\mathrm{M}} = \gamma_0 H_z$, $f_{\mathrm{M}} = -\gamma_\tau \boldsymbol{E}$, and $v_{\mathrm{c}} = \int_\Gamma \gamma_\Gamma \boldsymbol{E}\, \mathrm{d}s$. The boundary power is

$$\langle f_{\mathrm{M}}, e_{\mathrm{M}}\rangle_{\partial\Omega} + v_{\mathrm{c}} i_{\mathrm{c}}.$$

The perfectly electric boundary condition is $f_{\mathrm{M}} = 0$, that is, $\gamma_\tau \boldsymbol{E} = 0$. The perfectly magnetic boundary condition is $e_{\mathrm{M}} = 0$, that is, $\gamma_0 H_z = 0$. Both conditions define maximally power-conserving Maxwell boundary relations.

More generally, let $K_{\mathrm{M}} : H^{1/2}(\partial\Omega) \to H^{-1/2}(\partial\Omega)$ be bounded and nonnegative in the sense that $\langle K_{\mathrm{M}} e, e\rangle_{\partial\Omega} \ge 0$ for all $e \in H^{1/2}(\partial\Omega)$. Then the graph relation $f_{\mathrm{M}} = -K_{\mathrm{M}} e_{\mathrm{M}}$ is maximally dissipative and defines a dissipative Maxwell boundary closure.

For a constant impedance parameter $\eta > 0$, the Silver–Müller condition is obtained by choosing $K_{\mathrm{M}} = \eta^{-1} \jmath$, where $\jmath : H^{1/2}(\partial\Omega) \to H^{-1/2}(\partial\Omega)$ denotes the canonical pivot embedding, characterized by $\langle \jmath e, \widetilde{e}\rangle_{\partial\Omega} = (e, \widetilde{e})_{L^2(\partial\Omega)}$ for $e, \widetilde{e} \in H^{1/2}(\partial\Omega)$. For regular fields this gives $-\gamma_\tau \boldsymbol{E} = -\eta^{-1}\gamma_0 H_z$, which is precisely the Silver–Müller condition (1). The corresponding boundary power contribution is

$$\langle f_{\mathrm{M}}, e_{\mathrm{M}}\rangle_{\partial\Omega} = -\eta^{-1} \|\gamma_0 H_z\|^2_{L^2(\partial\Omega)} = -\eta \|E_\tau\|^2_{L^2(\partial\Omega)}$$

whenever the traces are sufficiently regular.
At the scalar cable port, the open-circuit closure is $i_{\mathrm{c}} = 0$, while the short-circuit closure is $v_{\mathrm{c}} = 0$. Both are maximally power-conserving. A resistive termination is described by $v_{\mathrm{c}} = -r_{\mathrm{c}} i_{\mathrm{c}}$ with $r_{\mathrm{c}} \geq 0$. Its cable power is $v_{\mathrm{c}} i_{\mathrm{c}} = -r_{\mathrm{c}} |i_{\mathrm{c}}|^2 \leq 0$.
Independent Maxwell and cable closures are represented by product relations. In particular, if Θ_{M} and Θ_{c} are maximally dissipative, then $\Theta = \Theta_{\mathrm{M}} \times \Theta_{\mathrm{c}}$ is maximally dissipative in $\mathcal{U} \times \mathcal{U}'$. The weak model from Subsection 2.3 corresponds to the Silver–Müller Maxwell closure together with the open-circuit cable closure.

4.3. **Energy variables and internal damping**

We now incorporate the material coefficients. Assume that $L \in L^\infty(\Gamma)$ and $\mu, \varepsilon \in L^\infty(\Omega)$ are uniformly positive, and that $R \in L^\infty(\Gamma)$ and $\sigma \in L^\infty(\Omega)$ are nonnegative. On $\mathcal{X} = L^2(\Gamma) \times L^2(\Omega) \times L^2(\Omega)^2$ define

$$\mathcal{M} := \begin{bmatrix} L & 0 & 0 \\ 0 & \mu & 0 \\ 0 & 0 & \varepsilon \end{bmatrix}, \qquad \mathcal{R} := \begin{bmatrix} R & 0 & 0 \\ 0 & 0 & 0 \\ 0 & 0 & \sigma \end{bmatrix}.$$

Then $\mathcal{M}$ is bounded, self-adjoint, uniformly positive, and boundedly invertible, while $\mathcal{R}$ is bounded, self-adjoint, and positive semidefinite.
The energy inner product is $(x, \widetilde{x})_{\mathcal{M}} := (\mathcal{M}x, \widetilde{x})_{\mathcal{X}}$. It induces an equivalent Hilbert space structure on $\mathcal{X}$, which we denote by $\mathcal{X}_{\mathcal{M}}$. The corresponding Hamiltonian is

$$\mathcal{H}(x) := \tfrac{1}{2}\|x\|_{\mathcal{M}}^2 = \tfrac{1}{2}\|\sqrt{L} I\|_\Gamma^2 + \tfrac{1}{2}\|\sqrt{\mu} H_z\|_\Omega^2 + \tfrac{1}{2}\|\sqrt{\varepsilon}\boldsymbol{E}\|_\Omega^2.$$

For a closed boundary relation Θ, define the physical realization

$$\mathcal{G}_\Theta := \mathcal{M}^{-1}(\mathcal{J}_\Theta - \mathcal{R}), \qquad \mathrm{dom}(\mathcal{G}_\Theta) = \mathrm{dom}(\mathcal{J}_\Theta).$$

Thus the autonomous evolution equation is $\mathcal{M}\dot{x} = (\mathcal{J}_\Theta - \mathcal{R})x$.
For $x \in \mathrm{dom}(\mathcal{G}_\Theta)$, the Green identity gives

$$(\mathcal{G}_\Theta x, x)_{\mathcal{M}} = \langle \mathfrak{B}_2 x, \mathfrak{B}_1 x \rangle_{\mathcal{U}',\mathcal{U}} - \|\sqrt{R} I\|_\Gamma^2 - \|\sqrt{\sigma}\boldsymbol{E}\|_\Omega^2.$$

Consequently, $\mathcal{G}_\Theta$ is dissipative on $\mathcal{X}_{\mathcal{M}}$ whenever Θ is dissipative.

4.4. **Semigroup and group generation**

We now prove well-posedness of the autonomous continuous system.

Theorem 4.2. *Assume the geometric trace setting of Paragraph 1.2. Let $L \in L^\infty(\Gamma)$ and $\mu, \varepsilon \in L^\infty(\Omega)$ be uniformly positive, and let $R \in L^\infty(\Gamma)$ and $\sigma \in L^\infty(\Omega)$ be nonnegative. Let $\Theta \subset \mathcal{U} \times \mathcal{U}'$ be a maximally dissipative linear relation. Then*

$$\mathcal{G}_\Theta = \mathcal{M}^{-1}(\mathcal{J}_\Theta - \mathcal{R}), \qquad \mathrm{dom}(\mathcal{G}_\Theta) = \mathrm{dom}(\mathcal{J}_\Theta),$$

is maximally dissipative on $\mathcal{X}_{\mathcal{M}}$.
Consequently, $\mathcal{G}_\Theta$ generates a strongly continuous contraction semigroup on $\mathcal{X}_{\mathcal{M}}$.

Proof. By Theorem 4.1, $\mathcal{J}_\Theta$ is maximally dissipative on $\mathcal{X}$. First consider the lossless weighted operator

$$\mathcal{G}_\Theta^0 := \mathcal{M}^{-1}\mathcal{J}_\Theta, \qquad \mathrm{dom}(\mathcal{G}_\Theta^0) = \mathrm{dom}(\mathcal{J}_\Theta).$$

It is dissipative on $\mathcal{X}_\mathcal{M}$, since

$$(\mathcal{G}_\Theta^0 x, x)_\mathcal{M} = (\mathcal{J}_\Theta x, x)_\mathcal{X} \le 0 \quad \text{for all } x \in \operatorname{dom}(\mathcal{J}_\Theta).$$

We claim that $\mathcal{G}_\Theta^0$ is maximally dissipative on $\mathcal{X}_\mathcal{M}$. We use the following resolvent argument. Let A be a maximally dissipative operator on $\mathcal{X}$ and let $\mathcal{M}$ be bounded, self-adjoint, uniformly positive, and boundedly invertible. Then $\mathcal{M}^{-1}A$, with domain $\operatorname{dom}(A)$, is maximally dissipative on $\mathcal{X}_\mathcal{M}$. Indeed, dissipativity follows from $(\mathcal{M}^{-1}Ax, x)_\mathcal{M} = (Ax, x)_\mathcal{X} \le 0$.
It remains to prove the range condition. Let $\lambda > 0$ and $f \in \mathcal{X}$. We have to solve $(\lambda \operatorname{id}_\mathcal{X} - \mathcal{M}^{-1}A)x = f$, or equivalently $(\lambda\mathcal{M} - A)x = \mathcal{M}f$. Choose $\mu \ge \lambda\|\mathcal{M}\|_{\mathcal{L}(\mathcal{X})}$. Since A is maximally dissipative on $\mathcal{X}$, the resolvent $(\mu \operatorname{id}_\mathcal{X} - A)^{-1}$ exists and satisfies

$$\|(\mu \operatorname{id}_\mathcal{X} - A)^{-1}\|_{\mathcal{L}(\mathcal{X})} \le \tfrac{1}{\mu}.$$

The equation above is equivalent to the fixed-point problem

$$x = (\mu \operatorname{id}_\mathcal{X} - A)^{-1}\big(\mathcal{M}f + (\mu \operatorname{id}_\mathcal{X} - \lambda\mathcal{M})x\big).$$

Since $\mathcal{M}$ is self-adjoint and uniformly positive, there is $m > 0$ such that $\mathcal{M} \ge m \operatorname{id}_\mathcal{X}$. Hence

$$\|\mu \operatorname{id}_\mathcal{X} - \lambda\mathcal{M}\|_{\mathcal{L}(\mathcal{X})} \le \mu - \lambda m < \mu.$$

Thus the right-hand side is a contraction on $\mathcal{X}$. Consequently, $\operatorname{ran}(\lambda \operatorname{id}_\mathcal{X} - \mathcal{M}^{-1}A) = \mathcal{X}$. The range characterization of maximal dissipativity yields maximal dissipativity of $\mathcal{M}^{-1}A$ on $\mathcal{X}_\mathcal{M}$.
Applying this to $A = \mathcal{J}_\Theta$ shows that $\mathcal{G}_\Theta^0$ is maximally dissipative on $\mathcal{X}_\mathcal{M}$.
Next set $\mathcal{D} := \mathcal{M}^{-1}\mathcal{R}$. Then $\mathcal{D}$ is bounded on $\mathcal{X}_\mathcal{M}$. Moreover,

$$(-\mathcal{D}x, x)_\mathcal{M} = -(\mathcal{R}x, x)_\mathcal{X} \le 0 \quad \text{for all } x \in \mathcal{X},$$

because $\mathcal{R}$ is positive semidefinite on $\mathcal{X}$. Hence $-\mathcal{D}$ is a bounded dissipative operator on $\mathcal{X}_\mathcal{M}$. By the bounded dissipative perturbation theorem [16, Chap. III, Thm. 2.7],

$$\mathcal{G}_\Theta = \mathcal{G}_\Theta^0 - \mathcal{D} = \mathcal{M}^{-1}(\mathcal{J}_\Theta - \mathcal{R})$$

is maximally dissipative on $\mathcal{X}_\mathcal{M}$. The Lumer–Phillips theorem therefore implies that $\mathcal{G}_\Theta$ generates a strongly continuous contraction semigroup on $\mathcal{X}_\mathcal{M}$. □

For power-conserving boundary conditions and vanishing internal damping, one obtains reversible dynamics.

Theorem 4.3. *Assume the geometric trace setting of Paragraph 1.2 and the material assumptions of Theorem 4.2. Let Θ be maximally power-conserving. Then $\mathcal{G}_\Theta^0 = \mathcal{M}^{-1}\mathcal{J}_\Theta$ is skew-adjoint on $\mathcal{X}_\mathcal{M}$ and generates a strongly continuous isometric group.*
For every bounded nonnegative internal damping operator $\mathcal{R}$ of the form introduced in Subsection 4.3, the operator $\mathcal{G}_\Theta = \mathcal{G}_\Theta^0 - \mathcal{M}^{-1}\mathcal{R}$ generates a strongly continuous group. Its restriction to nonnegative times is a contraction semigroup. Unless $\mathcal{R} = 0$, the group is in general not isometric.

Proof. By Theorem 4.1, $\mathcal{J}_\Theta$ is skew-adjoint on $\mathcal{X}$. Hence $\mathcal{G}_\Theta^0 = \mathcal{M}^{-1}\mathcal{J}_\Theta$ is skew-adjoint on $\mathcal{X}_\mathcal{M}$. Indeed, the passage from $\mathcal{J}_\Theta$ on $\mathcal{X}$ to $\mathcal{G}_\Theta^0$ on $\mathcal{X}_\mathcal{M}$ is precisely the change from the reference inner product to the energy inner product:

$$(\mathcal{G}_\Theta^0 x, \widetilde{x})_\mathcal{M} = (\mathcal{J}_\Theta x, \widetilde{x})_\mathcal{X} = -(x, \mathcal{J}_\Theta \widetilde{x})_\mathcal{X} = -(x, \mathcal{G}_\Theta^0 \widetilde{x})_\mathcal{M}$$

for all $x, \widetilde{x} \in \operatorname{dom}(\mathcal{J}_\Theta)$, and the adjoint domains correspond under the same change of inner product. Therefore $\mathcal{G}_\Theta^0$ generates a strongly continuous isometric group.
Since $\mathcal{M}^{-1}\mathcal{R}$ is bounded on $\mathcal{X}_\mathcal{M}$, the bounded perturbation theorem for group generators implies that $\mathcal{G}_\Theta$ also generates a strongly continuous group. Since a maximally power-conserving relation is in particular maximally dissipative, the forward semigroup is contractive by Theorem 4.2. □

For every classical solution of $\dot{x} = \mathcal{G}_\Theta x$, the Hamiltonian satisfies

$$\tfrac{\mathrm{d}}{\mathrm{d}t}\mathcal{H}(x(t)) = \langle \mathfrak{B}_2 x(t), \mathfrak{B}_1 x(t)\rangle_{\mathcal{U}',\mathcal{U}} - \|\sqrt{R}I(t)\|_\Gamma^2 - \|\sqrt{\sigma}\boldsymbol{E}(t)\|_\Omega^2.$$

For the Silver–Müller boundary condition and the open-circuit cable closure this becomes, for sufficiently regular solutions,

$$\tfrac{\mathrm{d}}{\mathrm{d}t}\mathcal{H}(x(t)) = -\eta\|E_\tau(t)\|_{L^2(\partial\Omega)}^2 - \|\sqrt{R}I(t)\|_\Gamma^2 - \|\sqrt{\sigma}\boldsymbol{E}(t)\|_\Omega^2.$$

Finally, an impressed current density can be included as a distributed input. The forced system takes the form

$$\dot{x}(t) = \mathcal{G}_\Theta x(t) - \mathcal{M}^{-1}\begin{bmatrix} 0 \\ 0 \\ \boldsymbol{J}_0(t) \end{bmatrix}.$$

For classical solutions, the Hamiltonian balance then contains the additional power term $-(\boldsymbol{E}(t), \boldsymbol{J}_0(t))_\Omega$.

Remark 4.4 (Cable endpoint actuation)**.** We now comment on possible actuation through the cable endpoint port. The outer Maxwell boundary relation remains homogeneous and represents the passive exterior termination of the computational domain. The following discussion concerns only inhomogeneous data at the scalar cable endpoint port.

In the full telegrapher model, before imposing open-circuit endpoint conditions, the line contribution to the boundary power is $V(t,0)I(t,0) - V(t,\ell)I(t,\ell)$. If the two endpoint currents are identified with one terminal current $i_\mathrm{c}(t)$, this contribution becomes

$$\big(V(t,0) - V(t,\ell)\big)i_\mathrm{c}(t).$$

Using the coupling relation $\gamma_\Gamma \boldsymbol{E} = -\partial_s V$, the conjugate terminal voltage is

$$v_\mathrm{c}(t) = \int_\Gamma \gamma_\Gamma \boldsymbol{E}(t)\,\mathrm{d}s = V(t,0) - V(t,\ell).$$

Thus $i_\mathrm{c} = 0$ is the homogeneous open-circuit closure used above, whereas endpoint actuation would formally correspond to prescribing $i_\mathrm{c}(t) = i_\mathrm{in}(t)$, prescribing $v_\mathrm{c}(t) = v_\mathrm{in}(t)$, or imposing an affine terminal relation such as

$$v_\mathrm{c}(t) = -r_\mathrm{c} i_\mathrm{c}(t) + v_\mathrm{in}(t), \qquad r_\mathrm{c} \geq 0.$$

The endpoint-actuated formulations above can be treated within the standard system-node framework for boundary control systems: the prescribed scalar endpoint quantity is regarded as a boundary input, and the conjugate cable-port quantity as the associated output. Let $x_0 = (I_0, H_{z,0}, \boldsymbol{E}_0)$ be the initial state. The corresponding compatibility condition means that $x_0 \in \mathrm{dom}(\mathcal{J}_\mathrm{max})$, that x_0 satisfies the chosen homogeneous outer Maxwell boundary relation, and that the prescribed cable endpoint relation holds at $t = 0$. Thus, for current actuation one requires $i_\mathrm{c}(x_0) = i_\mathrm{in}(0)$, for voltage actuation one requires $v_\mathrm{c}(x_0) = v_\mathrm{in}(0)$, and for the affine resistive termination $v_\mathrm{c}(t) = -r_\mathrm{c} i_\mathrm{c}(t) + v_\mathrm{in}(t)$ one requires $v_\mathrm{c}(x_0) + r_\mathrm{c} i_\mathrm{c}(x_0) = v_\mathrm{in}(0)$. If the corresponding scalar endpoint input belongs to $W^{2,1}(0,T)$ and this compatibility condition is satisfied, then the system-node formulation yields existence of a classical solution. This follows, as in the related three-dimensional Maxwell–cable model, from the solution theory for system nodes in Staffans; see [20, Thm. 4.3.9] and [14, Sec. 5]. We do not carry out the analogous system-node construction for the present reduced model here. ◇

5. Structure-preserving discretization

We now pass to a structure-preserving discretization of the coupled field-line model. The construction is carried out in two steps. We first discretize in time by the implicit midpoint rule and record the corresponding discrete power balance. The compatible finite element discretization is then introduced in the following subsections.

5.1. **Implicit midpoint rule**

We consider the port-Hamiltonian weak formulation (8) on the time interval $[0,T]$. Let $0 = t_0 < t_1 < \cdots < t_N = T$ be a uniform partition with time step $\Delta t = t_{n+1} - t_n$ and midpoint $t_{n+1/2} = t_n + \Delta t/2$. For a sequence $(U_n)_{n=0}^N$ in Z we write

$$\delta_t U_{n+1/2} := \frac{U_{n+1} - U_n}{\Delta t}, \qquad U_{n+1/2} := \frac{U_{n+1} + U_n}{2}.$$

Here, as in Subsection 2.4, the state is ordered as $U = [I; \boldsymbol{E}; H_z]$.
Given $U_n \in Z$, the implicit midpoint step consists in finding $U_{n+1} \in Z$ such that

$$M(W, \delta_t U_{n+1/2}) = J(W, U_{n+1/2}) - Q(W, U_{n+1/2}) - B_{n+1/2}(W) \tag{11}$$

for all $W \in Z$, where $B_{n+1/2}(W) := (\boldsymbol{\phi}, \boldsymbol{J}_0(t_{n+1/2}))_\Omega$ for $W = [p; \boldsymbol{\phi}; \psi]$. Thus all storage, interconnection, dissipation, and source terms are evaluated at the midpoint.
The time-discrete Hamiltonian is

$$\mathcal{H}_n := \tfrac{1}{2} M(U_n, U_n) = \tfrac{1}{2}\|\sqrt{L} I_n\|_\Gamma^2 + \tfrac{1}{2}\|\sqrt{\varepsilon}\boldsymbol{E}_n\|_\Omega^2 + \tfrac{1}{2}\|\sqrt{\mu} H_{z,n}\|_\Omega^2.$$

Choosing $W = U_{n+1/2}$ in (11) and using the skew-symmetry of J gives

$$M(U_{n+1/2}, \delta_t U_{n+1/2}) = -Q(U_{n+1/2}, U_{n+1/2}) - B_{n+1/2}(U_{n+1/2}).$$

By symmetry of M,

$$M(U_{n+1/2}, \delta_t U_{n+1/2}) = \frac{\mathcal{H}_{n+1} - \mathcal{H}_n}{\Delta t}.$$

Hence the midpoint rule satisfies the exact discrete power balance

$$\frac{\mathcal{H}_{n+1} - \mathcal{H}_n}{\Delta t} + Q(U_{n+1/2}, U_{n+1/2}) = -B_{n+1/2}(U_{n+1/2}).$$

In particular, in the lossless and source-free case $Q = 0$ and $B_{n+1/2} = 0$, the Hamiltonian is preserved exactly: $\mathcal{H}_{n+1} = \mathcal{H}_n$ for all n.
If the midpoint rule is applied after imposing a maximally dissipative boundary closure Θ, then the abstract time step can equivalently be written on the energy space $\mathcal{X}_\mathcal{M}$ as

$$\left(\mathrm{id}_\mathcal{X} - \frac{\Delta t}{2}\mathcal{G}_\Theta\right) x_{n+1} = \left(\mathrm{id}_\mathcal{X} + \frac{\Delta t}{2}\mathcal{G}_\Theta\right) x_n + \Delta t\, g_{n+1/2},$$

with the corresponding midpoint source term $g_{n+1/2}$. Since $\mathcal{G}_\Theta$ is maximally dissipative by Theorem 4.2, the operator $\mathrm{id}_\mathcal{X} - (\Delta t/2)\mathcal{G}_\Theta$ is bijective for every $\Delta t > 0$. Thus the implicit midpoint step is well-defined at the operator level for every time step.

5.2. **Compatible finite element spaces**

We now introduce a compatible finite element discretization of the midpoint scheme. Let $\mathcal{T}_h$ be a conforming triangulation of Ω. We assume that the embedded line Γ is resolved by the mesh, that is, Γ is the union of a finite number of mesh edges. This assumption ensures that the tangential trace of the discrete electric field can be evaluated on Γ without an additional projection.
The discrete state space is

$$Z_h := P_0(\Gamma) \times N_1(\Omega) \times P_0(\Omega),$$

where $P_0(\Gamma)$ denotes the space of elementwise constants on the line mesh, $P_0(\Omega)$ denotes the space of elementwise constants on $\mathcal{T}_h$, and $N_1(\Omega)$ is the lowest-order Nédélec edge element space. Thus the current, electric field, and magnetic field are approximated as

$$I^h = \sum_{\alpha=1}^{M_I} i_\alpha p_\alpha, \qquad \boldsymbol{E}^h = \sum_{\alpha=1}^{M_E} e_\alpha \boldsymbol{w}_\alpha, \qquad H_z^h = \sum_{\alpha=1}^{M_H} h_\alpha q_\alpha.$$

Here (p_α), $(\boldsymbol{w}_\alpha)$, and (q_α) are bases of $P_0(\Gamma)$, $N_1(\Omega)$, and $P_0(\Omega)$, respectively. The coefficient vectors are denoted by $\mathbf{i} \in \mathbb{R}^{M_I}$, $\mathbf{e} \in \mathbb{R}^{M_E}$, and $\mathbf{h} \in \mathbb{R}^{M_H}$, and the full discrete state vector is

$$\mathbf{U} := \begin{bmatrix} \mathbf{i} \\ \mathbf{e} \\ \mathbf{h} \end{bmatrix} \in \mathbb{R}^{M_I+M_E+M_H}.$$

Since $N_1(\Omega) \subset H(\mathrm{curl}, \Omega)$ and the line is aligned with mesh edges, the tangential component of every $\boldsymbol{E}^h \in N_1(\Omega)$ has a well-defined L^2 restriction to Γ. In particular, the coupling trace is represented directly by the edge degrees of freedom belonging to the edges on Γ. This gives the compatible discrete diagram

$$P_0(\Gamma) \xleftarrow{\gamma_\Gamma^h} N_1(\Omega) \xrightarrow{\nabla\times} P_0(\Omega).$$

Thus the electric field space is the central compatibility space: the discrete curl maps it to the magnetic field space, while the discrete tangential trace maps it to the current space on the embedded line.

5.3. **Finite-dimensional port-Hamiltonian formulation**

Restricting the bilinear forms M, J, and Q from Subsection 2.4 to Z_h gives a finite-dimensional port-Hamiltonian system. The storage matrices are defined by

$$(\mathbf{M}^L)_{\alpha\beta} := (p_\alpha, Lp_\beta)_\Gamma, \qquad (\mathbf{M}^\varepsilon)_{\alpha\beta} := (\boldsymbol{w}_\alpha, \varepsilon \boldsymbol{w}_\beta)_\Omega, \qquad (\mathbf{M}^\mu)_{\alpha\beta} := (q_\alpha, \mu q_\beta)_\Omega.$$

The dissipation matrices are

$$(\mathbf{M}^R)_{\alpha\beta} := (p_\alpha, Rp_\beta)_\Gamma, \quad (\mathbf{M}^\sigma)_{\alpha\beta} := (\boldsymbol{w}_\alpha, \sigma \boldsymbol{w}_\beta)_\Omega, \quad (\mathbf{Z}^\eta)_{\alpha\beta} := \langle \eta(\boldsymbol{w}_\alpha)_\tau, (\boldsymbol{w}_\beta)_\tau \rangle_{\partial\Omega}.$$

Finally, the discrete curl and field-line coupling matrices are

$$\mathbf{K}_{\alpha\beta} := (q_\alpha, \nabla \times \boldsymbol{w}_\beta)_\Omega, \qquad (\mathbf{C}_\Gamma)_{\alpha\beta} := (p_\alpha, \gamma_\Gamma^h \boldsymbol{w}_\beta)_\Gamma.$$

Here $\mathbf{K}$ maps electric degrees of freedom to magnetic test degrees of freedom, while $\mathbf{C}_\Gamma$ maps electric degrees of freedom to current test degrees of freedom on the line.
With the ordering $\mathbf{U} = [\mathbf{i}; \mathbf{e}; \mathbf{h}]$, the global mass, interconnection, and dissipation matrices are

$$\mathbf{M} = \begin{bmatrix} \mathbf{M}^L & 0 & 0 \\ 0 & \mathbf{M}^\varepsilon & 0 \\ 0 & 0 & \mathbf{M}^\mu \end{bmatrix}, \quad \mathbf{Q} = \begin{bmatrix} \mathbf{M}^R & 0 & 0 \\ 0 & \mathbf{M}^\sigma + \mathbf{Z}^\eta & 0 \\ 0 & 0 & 0 \end{bmatrix}, \quad \mathbf{J} = \begin{bmatrix} 0 & \mathbf{C}_\Gamma & 0 \\ -\mathbf{C}_\Gamma^\top & 0 & \mathbf{K}^\top \\ 0 & -\mathbf{K} & 0 \end{bmatrix}.$$

Thus $\mathbf{J} = -\mathbf{J}^\top$ by construction. The source vector acts only on the electric field equation. We write

$$\mathbf{B}_{\mathrm{src}} := \begin{bmatrix} 0 \\ \mathbf{I}_{M_E} \\ 0 \end{bmatrix}, \qquad (\mathbf{f}_{n+1/2})_\alpha := (\boldsymbol{w}_\alpha, \boldsymbol{J}_0(t_{n+1/2}))_\Omega.$$

The fully discrete midpoint scheme is therefore

$$\mathbf{M}\delta_t \mathbf{U}_{n+1/2} = (\mathbf{J}-\mathbf{Q})\overline{\mathbf{U}}_{n+1/2} - \mathbf{B}_{\mathrm{src}}\mathbf{f}_{n+1/2}, \tag{12}$$

where

$$\delta_t \mathbf{U}_{n+1/2} = \frac{\mathbf{U}_{n+1}-\mathbf{U}_n}{\Delta t}, \qquad \overline{\mathbf{U}}_{n+1/2} = \frac{\mathbf{U}_{n+1}+\mathbf{U}_n}{2}.$$

Equivalently, collecting the unknown time level on the left-hand side gives the linear system

$$\left(\mathbf{M} - \frac{\Delta t}{2}(\mathbf{J}-\mathbf{Q})\right)\mathbf{U}_{n+1} = \left(\mathbf{M} + \frac{\Delta t}{2}(\mathbf{J}-\mathbf{Q})\right)\mathbf{U}_n - \Delta t\,\mathbf{B}_{\mathrm{src}}\mathbf{f}_{n+1/2}. \tag{13}$$

5.4. **Discrete power balance and solvability**

The fully discrete system inherits the port-Hamiltonian structure of the continuous weak formulation. Indeed,

$$\mathbf{M} = \mathbf{M}^\top > 0, \qquad \mathbf{J} = -\mathbf{J}^\top, \qquad \mathbf{Q} = \mathbf{Q}^\top \geq 0.$$

The positive definiteness of $\mathbf{M}$ follows from the uniform positivity of L, ε, and μ. The nonnegativity of $\mathbf{Q}$ follows from the nonnegativity of R, σ, and η. The skew-symmetry of $\mathbf{J}$ is built into the block definition above and reflects the power-conserving field-line interconnection.

The discrete Hamiltonian is $\mathcal{H}_h(\mathbf{U}) := \frac{1}{2}\mathbf{U}^\top\mathbf{M}\mathbf{U}$. Multiplying (12) by $\overline{\mathbf{U}}_{n+1/2}^\top$ gives

$$\overline{\mathbf{U}}_{n+1/2}^\top \mathbf{M}\delta_t \mathbf{U}_{n+1/2} = -\overline{\mathbf{U}}_{n+1/2}^\top \mathbf{Q}\overline{\mathbf{U}}_{n+1/2} - \overline{\mathbf{e}}_{n+1/2}^\top \mathbf{f}_{n+1/2},$$

where $\overline{\mathbf{e}}_{n+1/2}$ denotes the electric part of $\overline{\mathbf{U}}_{n+1/2}$. Since $\mathbf{M}$ is symmetric,

$$\overline{\mathbf{U}}_{n+1/2}^\top \mathbf{M}\delta_t \mathbf{U}_{n+1/2} = \frac{\mathcal{H}_h(\mathbf{U}_{n+1}) - \mathcal{H}_h(\mathbf{U}_n)}{\Delta t}.$$

Therefore the fully discrete power balance is

$$\frac{\mathcal{H}_h(\mathbf{U}_{n+1}) - \mathcal{H}_h(\mathbf{U}_n)}{\Delta t} + \overline{\mathbf{U}}_{n+1/2}^\top \mathbf{Q}\overline{\mathbf{U}}_{n+1/2} = -\overline{\mathbf{e}}_{n+1/2}^\top \mathbf{f}_{n+1/2}. \tag{14}$$

In particular, in the lossless and source-free case, the discrete Hamiltonian is preserved exactly.

The linear system (13) is uniquely solvable for every $\Delta t > 0$. To see this, set

$$\mathbf{A}_{\Delta t} := \mathbf{M} - \frac{\Delta t}{2}(\mathbf{J}-\mathbf{Q}).$$

For every nonzero vector $\mathbf{x}$,

$$\mathbf{x}^\top \mathbf{A}_{\Delta t}\mathbf{x} = \mathbf{x}^\top \mathbf{M}\mathbf{x} + \frac{\Delta t}{2}\mathbf{x}^\top \mathbf{Q}\mathbf{x} > 0,$$

because the skew-symmetric part $\mathbf{J}$ does not contribute. Hence $\mathbf{A}_{\Delta t}$ is nonsingular.

Representation of magnetic jumps. The discontinuous space $P_0(\Omega)$ allows the scalar magnetic field to have jumps across element interfaces. For an interior edge e shared by two elements K^+ and K^-, the jump of $H_z^h \in P_0(\Omega)$ is

$$[\![H_z^h]\!]_e := H_z^h|_{K^+} - H_z^h|_{K^-}.$$

The transpose of the discrete curl matrix represents precisely these edge contributions in weak form. More explicitly, for an electric edge basis function $\boldsymbol{w}_\alpha$ supported around an interior edge, the quantity $(\mathbf{K}^\top\mathbf{h})_\alpha$ is the discrete analogue of the circulation contribution generated by the jumps of the piecewise constant magnetic

field. Along edges belonging to Γ, the additional term $-\mathbf{C}_\Gamma^\top \mathbf{i}$ in the electric equation represents the line-supported current. Thus the discrete electric equation contains the weak balance between magnetic jumps and line current. In this sense, the jump condition recovered in Proposition 3.3 is not imposed as an additional interface constraint; it is encoded in the variational coupling and in the algebraic adjointness of $\mathbf{C}_\Gamma$ and $\mathbf{C}_\Gamma^\top$.

Mesh-scale regularization of line singularities. A line-supported current is a lower-dimensional source term in the field equation. A volumetric finite element discretization cannot resolve the corresponding subgrid field behavior without resolving the physical conductor thickness. In the present formulation, the effect of the line current is regularized at the mesh scale: the current is represented in $P_0(\Gamma)$, and its action on the field is distributed through the edge degrees of freedom of $N_1(\Omega)$ that lie on Γ. The magnetic field $H_z^h \in P_0(\Omega)$ is therefore an elementwise averaged field. It does not approximate point values near the embedded line; instead, it represents the cell-wise magnetic energy induced by the line source. Consequently, the discrete magnetic energy remains finite for every fixed mesh, while the concentration of the field near the line can reappear under mesh refinement.

This interpretation is important for the numerical method. The filamentary model should not be read as a pointwise regular field model near Γ. Rather, it is a reduced model in which the singular conductor geometry has already been collapsed to a one-dimensional port. The compatible finite element discretization then regularizes this reduced model by replacing the unresolved near-line behavior by weak edge contributions. This is the mechanism that allows the method to combine line-supported currents with a standard two-dimensional field mesh.

Inter-element consistency. Although H_z^h is discontinuous, the electric field $\boldsymbol{E}^h \in N_1(\Omega)$ has single-valued tangential components across mesh edges. For each element $K \in \mathcal{T}_h$, the local identity

$$\int_K \mu \dot{H}_z^h = -\int_{\partial K} E_\tau^h$$

is the discrete form of Faraday's law. Thus the evolution of the piecewise constant magnetic field is driven by the circulation of a globally compatible tangential electric field. The line current enters only through the edge degrees of freedom on Γ and modifies the adjacent weak balance by the term $-\mathbf{C}_\Gamma^\top \mathbf{i}$. No penalty terms or artificial inter-element stabilization are needed to obtain either the jump representation or the discrete power balance.

6. Numerical experiments

We present numerical experiments that illustrate the behavior of the structure-preserving discretization developed in Section 5. The tests are designed to show the coupled field-line dynamics, the resulting radiation pattern, and the discrete power balance of the method.

6.1. **Problem setup**

We consider a disk-shaped computational domain Ω of radius 50 cm; see Figure 1(A). The embedded line represents a horizontally oriented half-wave dipole antenna excited through a feeding structure. The impressed current density in the source region is chosen as a horizontally polarized harmonic source,

$$\boldsymbol{J}_0(t) = [-\sin(2\pi f_{\mathrm{src}} t), 0]^\top, \qquad f_{\mathrm{src}} = 2.4 \text{ GHz}.$$

Both the waveguide conductors and the antenna are modeled as filamentary lines. Thus, the computational setting is a multi-line version of the field-line coupling described above; the corresponding operator-theoretic construction extends componentwise as indicated in Remark 3.6.

The background medium is vacuum, with

$$\varepsilon_0 = 8.854 \cdot 10^{-12} \text{ F/m}, \qquad \mu_0 = 4\pi \cdot 10^{-7} \text{ H/m}, \qquad \sigma_0 = 0 \text{ S/m}.$$

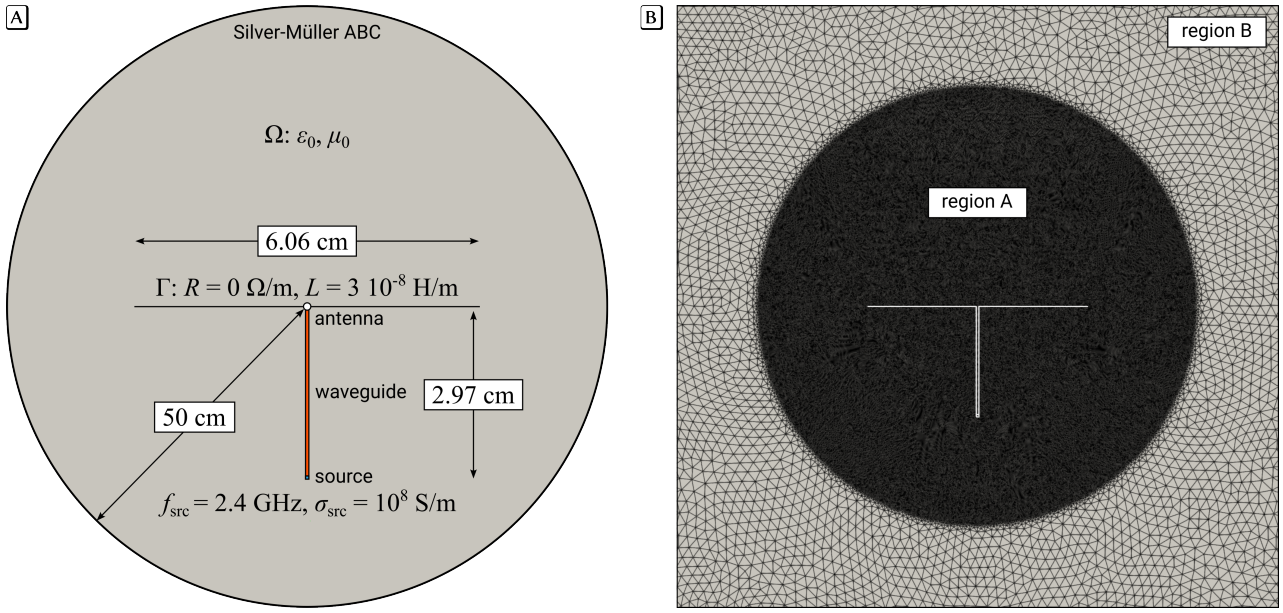

FIGURE 1. (A) Computational setting, including antenna geometry and material parameters. (B) Triangulation near the antenna, showing the extended reactive near-field region A and the radiating near- and far-field region B.

The source region is modeled as highly conducting material with the same permittivity and permeability and with $\sigma_{\mathrm{src}} = 10^8$ S/m. The line parameters used in the reduced model are $R = 0$ Ω/m and $L = 3 \cdot 10^{-8}$ H/m. The time step is chosen such that one source period $T_{\mathrm{src}} = 1/f_{\mathrm{src}}$ is resolved by 50 time steps. The simulation is run until $T = 20T_{\mathrm{src}}$. The computational mesh is split into an extended reactive near-field region A and a radiating near- and far-field region B; see Figure 1(B). The characteristic mesh sizes h_{A} and h_{B} are chosen such that the 0.06 cm feed gap is resolved by two elements and the wavelength is resolved by approximately 40 elements, that is, $\lambda_{\mathrm{src}} \approx 40h_{\mathrm{B}}$. The resulting mesh has minimum and maximum edge lengths $h_{\min} \approx 0.0002$ and $h_{\max} \approx 0.0046$ and leads to 1 203 424 degrees of freedom. The formulation is implemented in FreeFEM, and the linear systems are solved with UMFPACK.

The fields generated by the feeding source dominate the total field. To visualize the antenna contribution, we compute a background solution without the antenna and subtract it from the coupled field-line solution. Thus,

$$\boldsymbol{E}^{h,\mathrm{ant}} := \boldsymbol{E}^{h} - \boldsymbol{E}^{h,\mathrm{src}}, \qquad H_z^{h,\mathrm{ant}} := H_z^{h} - H_z^{h,\mathrm{src}}.$$

In the field plots we show the local magnitudes

$$E^{h,\mathrm{ant}} = \left(|E_x^{h,\mathrm{ant}}|^2 + |E_y^{h,\mathrm{ant}}|^2\right)^{1/2}, \qquad |H_z^{h,\mathrm{ant}}|.$$

6.2. **Radiation pattern**

Figure 2 shows the electric field strength of the antenna contribution. Figure 3 shows the corresponding magnetic field strength. The fields are scaled for visualization: the value "max" in each plot denotes the upper end of the color scale, and larger values are clipped.

At $t = 10T_{\mathrm{src}}$, the expected dipole-type radiation pattern is visible; see Figures 2(A) and 3(A). The detailed views in Figures 2(B) and 3(B) show the near-field behavior around the antenna. At the earlier time $t = 2T_{\mathrm{src}}$, the propagating wave is still mainly confined to the feeding structure; see Figures 2(C) and 3(C). In particular, the magnetic field plot shows the expected discontinuity across the embedded line.

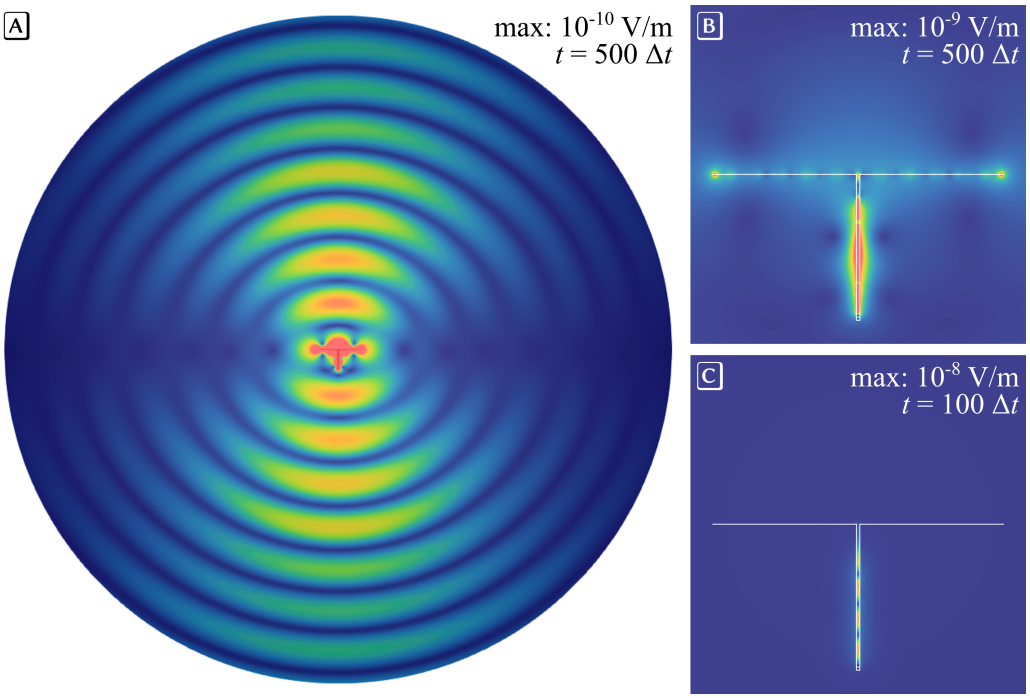

FIGURE 2. Electric field strength of the antenna contribution. (A), (B) $t = 10T_{\mathrm{src}}$; (C) $t = 2T_{\mathrm{src}}$. The value "max" denotes the upper end of the color scale.

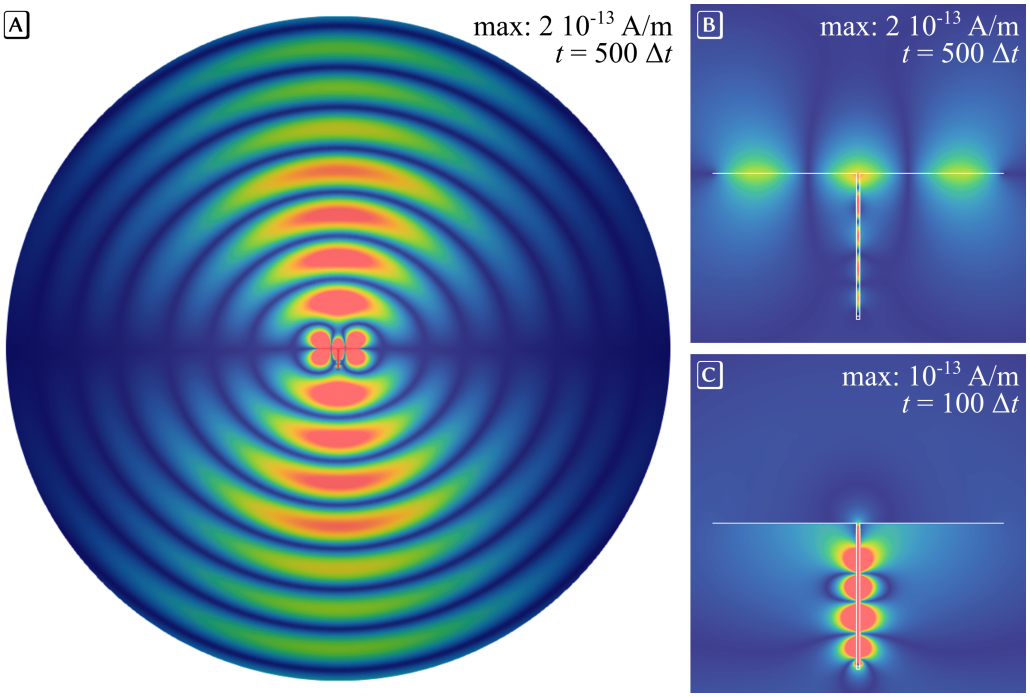

FIGURE 3. Magnetic field strength of the antenna contribution. (A), (B) $t = 10T_{\mathrm{src}}$; (C) $t = 2T_{\mathrm{src}}$. The value "max" denotes the upper end of the color scale.

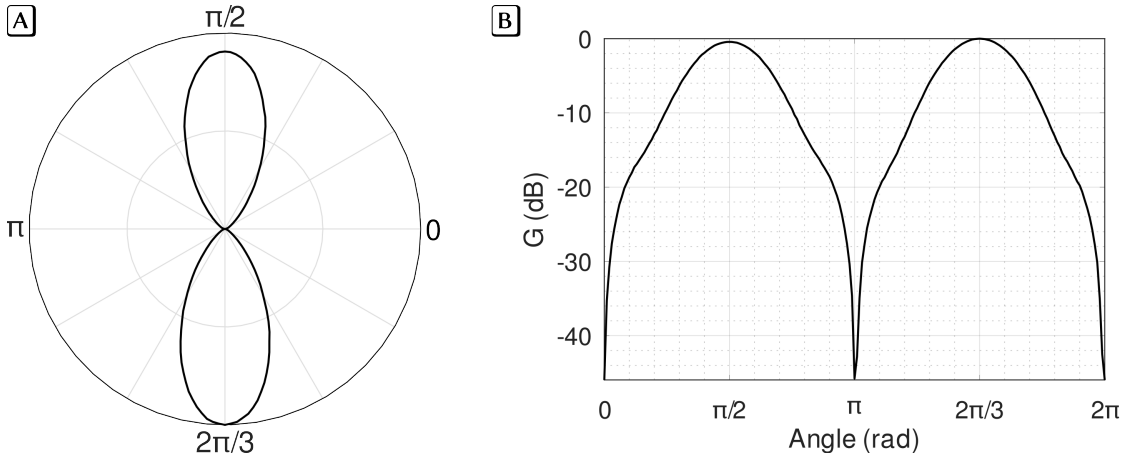

FIGURE 4. Radiation characteristics of the half-wave dipole antenna. (A) Polar plot of $\overline{S}_r(\theta)$. (B) Decibel representation $G(\theta)$.

To quantify the radiation pattern, we sample the Poynting vector

$$\boldsymbol{S} = \boldsymbol{E} \times \boldsymbol{H} = [E_y H_z, -E_x H_z]^\top$$

on the outer boundary. With the outward unit normal $\boldsymbol{n}(\theta) = [\cos\theta, \sin\theta]^\top$, the radial component is

$$S_n(t,\theta) = E_y(t,\theta) H_z(t,\theta) \cos\theta - E_x(t,\theta) H_z(t,\theta) \sin\theta.$$

We average this quantity over one source period, from $t_1 = 501\Delta t$ to $t_2 = 551\Delta t$, and normalize it according to

$$\overline{S}_r(\theta) = \frac{A}{T_{\mathrm{src}}} \int_{t_1}^{t_2} S_n(t,\theta)\,\mathrm{d}t, \qquad \max_\theta \overline{S}_r(\theta) = 1.$$

The decibel representation is

$$G(\theta) = 10 \log_{10} \overline{S}_r(\theta).$$

The resulting radiation pattern is shown in Figure 4. The asymmetry compared with an ideal half-wave dipole is caused by the feeding waveguide, which interacts with the antenna and modifies the otherwise symmetric radiation characteristics.

6.3. **Energy balance**

The considered configuration is dissipative. Energy is removed from the computational domain through ohmic losses in the highly conducting source region and through the Silver–Müller absorbing boundary condition. At the same time, the storage capacity of the configuration is small: most of the supplied energy is transported out of the domain rather than stored in the antenna region.
This behavior is visible in Figure 5, where the rate of change of the discrete Hamiltonian remains close to zero throughout the computation. More precisely, the simulation gives

$$|\delta_t \mathcal{H}_h| < 3 \cdot 10^{-23} \qquad \text{for all } t \in [0, T].$$

Thus, no artificial accumulation of discrete energy is observed.
Figure 6(A) shows the supplied and dissipated power. The numerical results are consistent with the physical picture of a radiating antenna: the injected energy is rapidly balanced by conductive and radiative dissipation.

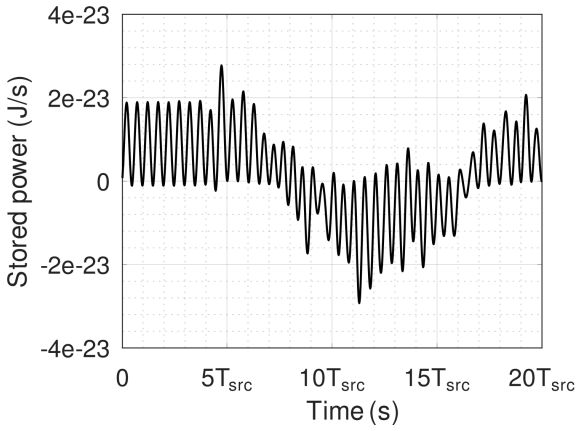

FIGURE 5. Rate of change of the discrete Hamiltonian as a function of time.

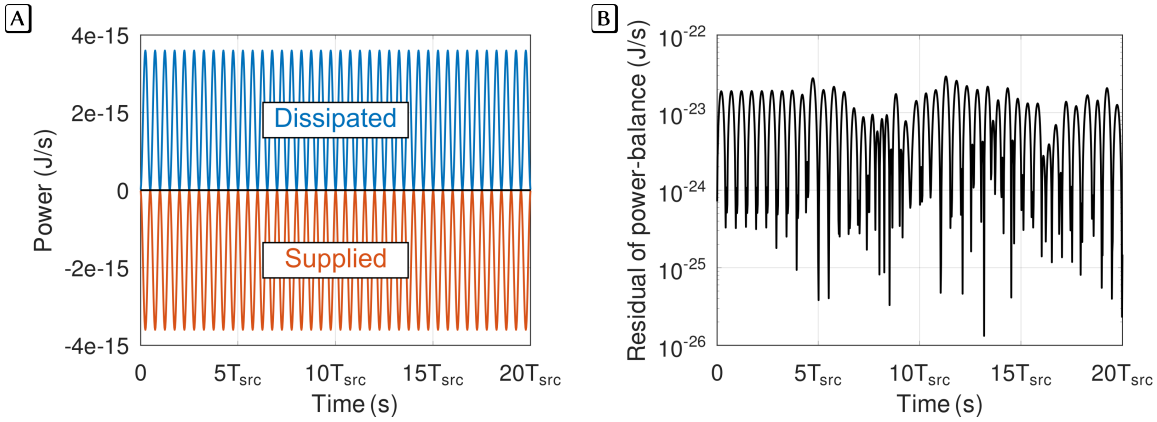

FIGURE 6. (A) Supplied and dissipated power as a function of time. (B) Residual of the discrete power balance.

6.4. **Verification of the discrete power balance**

As a verification of the structure-preserving discretization, we evaluate the residual of the fully discrete power balance (14). In the notation of Subsection 5.4, this residual is

$$r_n := \frac{\mathcal{H}_h(\mathbf{U}_{n+1}) - \mathcal{H}_h(\mathbf{U}_n)}{\Delta t} + \overline{\mathbf{U}}_{n+1/2}^{\top} \mathbf{Q} \overline{\mathbf{U}}_{n+1/2} + \overline{\mathbf{e}}_{n+1/2}^{\top} \mathbf{f}_{n+1/2}.$$

For an exact solve and exact quadrature, the residual vanishes up to round-off. In the present computation we observe

$$|r_n| < 10^{-22}$$

throughout the simulation; see Figure 6(B). This confirms that the implemented scheme reproduces the discrete power balance and does not introduce spurious numerical gain or loss of energy.

7. Conclusions

We have developed a structure-preserving formulation for the coupling of a two-dimensional electromagnetic field with reduced transmission-line models embedded in the field domain. The coupling is motivated by a distributed port that identifies the tangential electric field along the embedded line with the longitudinal voltage gradient of the line model. This leads to a reduced current-field formulation in which the field-line interaction is power-conserving, while material losses and absorbing boundary conditions enter as dissipative mechanisms.
A central part of the analysis is the operator-theoretic realization of the coupled lossless interconnection. Since the tangential restriction of an $H(\mathrm{curl},\Omega)$ field to an interior curve is not a bounded trace on the standard energy space, the interior tangential trace was introduced as a closed operator. The magnetic-field–cable block was then constructed as the adjoint of a minimal electric-field operator. This yields a closed maximal realization on the physical energy space and recovers, for regular states, the expected jump condition of the scalar magnetic field across the embedded line.
The associated Green identity leads to a boundary-triplet formulation that contains both the outer Maxwell port and the scalar cable port. Within this framework, conservative and dissipative boundary conditions are described by linear boundary relations. Maximally dissipative relations lead to maximally dissipative realizations of the physical generator and hence to strongly continuous contraction semigroups. In the lossless power-conserving case, the corresponding weighted realization generates an isometric group.
The discretization was designed to preserve the same structure at the finite-dimensional level. The implicit midpoint rule yields an exact time-discrete power balance for the quadratic Hamiltonian. In space, lowest-order Nédélec elements for the electric field and elementwise constants for the magnetic field and the line current form a compatible discretization. If the embedded line is aligned with mesh edges, the field-line coupling is represented directly by the tangential degrees of freedom. The resulting finite-dimensional system has a port-Hamiltonian form with a symmetric positive definite mass matrix, a skew-symmetric interconnection matrix, and a positive semidefinite dissipation matrix. Consequently, the fully discrete scheme satisfies an exact discrete power balance and is solvable for every time step.
The numerical experiments for a half-wave dipole antenna illustrate the coupled field-line dynamics and the radiation behavior of the method. The computed field patterns show the expected dipole-type radiation, while the discrete energy balance is satisfied up to round-off accuracy. This confirms the structure-preserving character of the implementation and shows that the method does not introduce spurious numerical gain or loss of energy.
Future work will address higher-order compatible discretizations, more general networks of embedded lines, and extensions to three-dimensional electromagnetic field-line systems. Another interesting direction is the treatment of exterior-domain radiation conditions within the same boundary-triplet and port-Hamiltonian framework.

Appendix A. Auxiliary analytic results

This appendix collects the technical analytic results used in the proofs. The notation is the one introduced in Section 1.

A.1. **Interior tangential trace and cable lifting**

Lemma A.1. *Let $\Omega \subset \mathbb{R}^2$ be a bounded Lipschitz domain and let $K \subset \Omega$ with $\overline{K} \subset \Omega$. Assume that the outer tangential trace $\gamma_\tau : H(\mathrm{curl},\Omega) \to H^{-1/2}(\partial\Omega)$ admits a bounded right inverse. Then, for every $f \in H^{-1/2}(\partial\Omega)$, there exists $\boldsymbol{E}_f \in H(\mathrm{curl},\Omega)$ such that $\gamma_\tau \boldsymbol{E}_f = f$ and such that the support of $\boldsymbol{E}_f$ is separated from K.*

Proof. Let $\mathcal{E}_\tau : H^{-1/2}(\partial\Omega) \to H(\mathrm{curl},\Omega)$ be a bounded right inverse of γ_τ. Since $\overline{K} \subset \Omega$, there exists a function $\chi \in W^{1,\infty}(\Omega)$ such that $\chi = 1$ in a neighborhood of $\partial\Omega$ and $\chi = 0$ in a neighborhood of K. Define $\boldsymbol{E}_f := \chi\,\mathcal{E}_\tau f$. Then $\boldsymbol{E}_f \in H(\mathrm{curl},\Omega)$, since multiplication by a $W^{1,\infty}$ function preserves $H(\mathrm{curl},\Omega)$. Moreover, $\chi = 1$ near $\partial\Omega$, and therefore $\gamma_\tau \boldsymbol{E}_f = \gamma_\tau(\mathcal{E}_\tau f) = f$. Finally, since $\chi = 0$ in a neighborhood of K, the support of $\boldsymbol{E}_f$ is separated from K. □

Lemma A.2. *Assume that Ω and Γ satisfy the geometric hypotheses stated in Subsection 1.2. Then the operator*

$$\gamma_\Gamma^\circ : C^\infty(\overline{\Omega})^2 \subset H(\mathrm{curl},\Omega) \longrightarrow L^2(\Gamma), \qquad \gamma_\Gamma^\circ \boldsymbol{E} = (\boldsymbol{E}|_\Gamma)\cdot \boldsymbol{\tau}_\Gamma,$$

is closable as an operator from $H(\mathrm{curl},\Omega)$ to $L^2(\Gamma)$.

Proof. Let $(\boldsymbol{E}_n)_{n\in\mathbb{N}} \subset C^\infty(\overline{\Omega})^2$ satisfy $\boldsymbol{E}_n \to 0$ in $H(\mathrm{curl},\Omega)$, and $\gamma_\Gamma^\circ \boldsymbol{E}_n \to g$ in $L^2(\Gamma)$. We show that $g = 0$. For $\varepsilon \in (0,\ell/2)$ set $\Gamma_\varepsilon := \gamma((\varepsilon,\ell-\varepsilon))$. By the tubular-neighborhood assumption, Γ_ε is a relatively open part of the boundary of a Lipschitz subdomain compactly contained in Ω. The standard tangential trace theorem applied to this subdomain gives $\gamma_\Gamma^\circ \boldsymbol{E}_n|_{\Gamma_\varepsilon} \to 0$ in $H^{-1/2}(\Gamma_\varepsilon)$. On the other hand, convergence in $L^2(\Gamma)$ implies that $\gamma_\Gamma^\circ \boldsymbol{E}_n|_{\Gamma_\varepsilon} \to g|_{\Gamma_\varepsilon}$ in $L^2(\Gamma_\varepsilon) \hookrightarrow H^{-1/2}(\Gamma_\varepsilon)$. Hence $g|_{\Gamma_\varepsilon} = 0$. Since $\varepsilon \in (0,\ell/2)$ was arbitrary and the endpoints of Γ have one-dimensional measure zero, it follows that $g = 0$ in $L^2(\Gamma)$. Thus γ_Γ° is closable. □

Proposition A.3. *Assume that Ω and Γ satisfy the geometric hypotheses stated in Subsection 1.2, and let γ_Γ be the closure of γ_Γ° from Lemma A.2. Then there exists a bounded operator $\mathcal{L}_\Gamma : L^2(\Gamma) \longrightarrow H_\Gamma(\mathrm{curl},\Omega)$ such that $\gamma_\Gamma \mathcal{L}_\Gamma g = g$, $\nabla \times \mathcal{L}_\Gamma g = 0$, and $\gamma_\tau \mathcal{L}_\Gamma g = 0$ for every $g \in L^2(\Gamma)$.*

Proof. We identify $g \in L^2(\Gamma)$ with a function on $(0,\ell)$ and set

$$(Pg)(s) := \int_0^s g(r)\,\mathrm{d}r.$$

Then $Pg \in H^1(0,\ell)$, $\partial_s Pg = g$, and $\|Pg\|_{H^1(0,\ell)} \le c\|g\|_{L^2(\Gamma)}$. Extend Pg boundedly to an element of $H^1(-\delta,\ell+\delta)$. Choose cut-off functions $\alpha \in C_c^\infty(-\delta,\ell+\delta)$ and $\beta \in C_c^\infty(-\rho,\rho)$ such that $\alpha = 1$ on $[0,\ell]$ and $\beta = 1$ near 0. In tubular coordinates define

$$\Phi_g(\Psi(s,r)) := \alpha(s)\beta(r)(Pg)(s),$$

and extend Φ_g by zero to Ω. Then $\Phi_g \in H_0^1(\Omega)$, its support is contained in U_Γ, and

$$\|\Phi_g\|_{H^1(\Omega)} \le c\|g\|_{L^2(\Gamma)}.$$

Set $\mathcal{L}_\Gamma g := \nabla\Phi_g$. Since $\Phi_g \in H_0^1(\Omega)$ has compact support away from $\partial\Omega$, we have $\gamma_\tau \mathcal{L}_\Gamma g = 0$. Furthermore, $\nabla \times \mathcal{L}_\Gamma g = \nabla \times \nabla\Phi_g = 0$ in the distributional sense. For smooth g, the construction in the tubular coordinates gives the tangential identity

$$(\nabla\Phi_g)\cdot\boldsymbol{\tau}_\Gamma = \partial_s(Pg) = g \qquad \text{on } \Gamma.$$

By a standard smoothing argument in the tubular coordinates and by the definition of the closed trace, this implies $\nabla\Phi_g \in H_\Gamma(\mathrm{curl},\Omega)$ and $\gamma_\Gamma\nabla\Phi_g = g$ for smooth g.
For general $g \in L^2(\Gamma)$ choose $g_n \in C^\infty([0,\ell])$ with $g_n \to g$ in $L^2(\Gamma)$ and let Φ_{g_n} be the corresponding potentials. The construction above gives

$$\nabla\Phi_{g_n} \to \nabla\Phi_g \quad \text{in } H(\mathrm{curl},\Omega), \qquad \gamma_\Gamma\nabla\Phi_{g_n} = g_n \to g \quad \text{in } L^2(\Gamma).$$

Since γ_Γ is closed, it follows that $\nabla\Phi_g \in H_\Gamma(\mathrm{curl},\Omega)$ and $\gamma_\Gamma\nabla\Phi_g = g$. The preceding estimates imply $\|\mathcal{L}_\Gamma g\|_{H_\Gamma(\mathrm{curl},\Omega)} \le c\|g\|_{L^2(\Gamma)}$. Thus $\mathcal{L}_\Gamma$ is bounded. □

References

[1] R. F. Harrington. *Field Computation by Moment Methods*. IEEE Press, Piscataway, NJ, 1993.
[2] C. A. Balanis. *Antenna Theory: Analysis and Design*. Wiley, Hoboken, NJ, 4 edition, 2016.
[3] C. R. Paul. *Analysis of Multiconductor Transmission Lines*. Wiley-IEEE Press, 2 edition, 2008.
[4] P. Monk. *Finite Element Methods for Maxwell's Equations*. Oxford University Press, Oxford, 2003.
[5] A. Bossavit. *Computational Electromagnetism: Variational Formulations, Complementarity, Edge Elements*. Academic Press, San Diego, 1998.

[6] D. N. Arnold, R. S. Falk, and R. Winther. Finite element exterior calculus, homological techniques, and applications. *Acta Numerica*, 15:1–155, 2006.
[7] R. Hiptmair. Finite elements in computational electromagnetism. *Acta Numerica*, 11:237–339, 2002.
[8] J.-C. Nédélec. Mixed finite elements in $\mathbb{R}^3$. *Numerische Mathematik*, 35:315–341, 1980.
[9] J.-C. Nédélec. A new family of mixed finite elements in $\mathbb{R}^3$. *Numerische Mathematik*, 50:57–81, 1986.
[10] D. Boffi, F. Brezzi, and M. Fortin. *Mixed Finite Element Methods and Applications*, volume 44 of *Springer Series in Computational Mathematics*. Springer, 2013.
[11] A. J. van der Schaft and B. M. Maschke. Hamiltonian formulation of distributed-parameter systems with boundary energy flow. *Journal of Geometry and Physics*, 42:166–194, 2002.
[12] B. Jacob and H. Zwart. *Linear Port-Hamiltonian Systems on Infinite-Dimensional Spaces*, volume 223 of *Operator Theory: Advances and Applications*. Birkhäuser, Basel, 2012.
[13] Ramy Rashad, Arjan J. van der Schaft, and Stefano Stramigioli. Twenty years of distributed port-hamiltonian systems: a literature review. *IMA J. Math. Control Inform.*, 37(4):1400–1422, 2020.
[14] Timo Reis and Nathanael Skrepek. Analysis of coupled Maxwell-cable problems. *J. Engrg. Math.*, 157(1), 2026.
[15] George J. Minty. A theorem on maximal monotonic sets in Hilbert space. *J. Math. Anal. Appl.*, 11(3):434–439, 1965.
[16] Klaus-Jochen Engel and Rainer Nagel. *One-Parameter Semigroups for Linear Evolution Equations*, volume 194 of *Graduate Texts in Mathematics*. Springer, New York, 2000.
[17] William McLean. *Strongly Elliptic Systems and Boundary Integral Equations*. Cambridge University Press, Cambridge, 2000.
[18] Jussi Behrndt, Mark M. Malamud, and Hagen Neidhardt. Scattering theory for open quantum systems with finite rank coupling. *Mathematical Physics, Analysis and Geometry*, 10(4):313–358, 2007.
[19] Sven-Ake Wegner. Boundary triplets for skew-symmetric operators and the generation of strongly continuous semigroups. *Anal. Math.*, 43(4):657–686, 2017.
[20] Olof J. Staffans. *Well-Posed Linear Systems*, volume 103 of *Encyclopedia of Mathematics and its Applications*. Cambridge University Press, Cambridge, 2005.